HHS Public Access

Author manuscript

Cell Host Microbe. Author manuscript; available in PMC 2018 October 11.

Published in final edited form as:

Cell Host Microbe. 2017 October 11; 22(4): 531–542.e8. doi:10.1016/j.chom.2017.08.009.

Dietary manganese promotes staphylococcal infection of the heart

Lillian J. Juttukonda[1], **Evelien T. M. Berends**[2], **Joseph P. Zackular**[1], **Jessica L. Moore**[3,4], **Matthew T. Stier**[1], **Yaofang Zhang**[4], **Jonathan E. Schmitz**[1], **William N. Beavers**[1], **Christiaan D. Wijers**[1], **Benjamin A. Gilston**[5,6], **Thomas E. Kehl-Fie**[7], **James Atkinson**[1], **Mary K. Washington**[1], **R. Stokes Peebles**[1,8], **Walter J. Chazin**[3,5,6], **Victor J. Torres**[2], **Richard M. Caprioli**[3,4,6], and **Eric P. Skaar**[1,*,#]

[1]Department of Pathology, Microbiology, and Immunology; Vanderbilt University Medical Center; Nashville TN 37232; USA

[2]Department of Microbiology, Microbial Pathogenesis Program; New York University School of Medicine; New York NY 10016; USA

[3]Department of Chemistry; Vanderbilt University; Nashville TN 37232; USA

[4]Mass Spectrometry Research Center; Vanderbilt University; Nashville TN 37232; USA

[5]Center for Structural Biology; Vanderbilt University; Nashville TN 37232; USA

[6]Department of Biochemistry; Vanderbilt University; Nashville TN 37232; USA

[7]Department of Microbiology; University of Illinois at Urbana-Champaign; Urbana IL 61801; USA

[8]Division of Allergy, Pulmonary and Critical Care Medicine, Department of Medicine; Vanderbilt University Medical Center; Nashville TN 37232; USA

Summary

Diet and specifically dietary metals can modify the risk of infection. However, the mechanisms by which manganese (Mn), a common dietary supplement, alters infection remain unexplored. We report that dietary Mn levels dictate the outcome of systemic infections caused by *Staphylococcus*

*Corresponding author information: Eric P. Skaar, PhD, MPH, Ernest Goodpasture Professor of Pathology, Vice Chair for Basic Research, Vanderbilt University Medical Center, 1161 21st Avenue South, MCN A-5102, Nashville, TN, 37232, Tel: 615-343-0002, Fax: 615-343-7392, eric.skaar@vanderbilt.edu.
#Lead Contact

Author Contributions

L.J.J. and E.P.S. designed the experiments and wrote the manuscript with input from co-authors. L.J.J. performed animal experiments, *in vitro* growth assays, flow cytometry experiments, bone marrow transplant experiments, cytokine analyses, and prepared samples for MS analyses. E.T.M.B. and V.J.T. designed and E.T.M.B. performed human neutrophil killing assays. J.P.Z. designed and carried out the microbiota and *C. difficile* experiment. J.L.M. cryosectioned all samples and performed MALDI IMS analyses with R.M.C. M.T.S. and R.S.P. assisted with bone marrow transplant experiments. Y.Z. and R.M.C. performed ICP-MS experiments. J.E.S. provided microbiological isolates. W.N.B. performed western blot analysis. C.D.W. assisted with growth assays. B.A.G. and W.J.C. purified recombinant calprotectin. T.K.F. performed the mouse experiments in Figure 4A and Supplementary Figure 3B. J.A. and M.K.W. assisted with histopathology analyses.

aureus, a leading cause of bacterial endocarditis. Mice fed a high Mn diet display alterations in Mn levels and localization within infected tissues, and *S. aureus* virulence and infection of the heart are enhanced. Although the canonical mammalian Mn-sequestering protein calprotectin surrounds staphylococcal heart abscesses, calprotectin is not released into the abscess nidus and does not limit Mn in this organ. Consequently, excess Mn is bioavailable to *S. aureus* in the heart. Bioavailable Mn is utilized by *S. aureus* to detoxify reactive oxygen species and protect against neutrophil killing, enhancing fitness within the heart. Therefore, a single dietary modification overwhelms vital host antimicrobial strategies, leading to fatal staphylococcal infection.

eTOC Blurb

Juttukonda et al. reveal that high dietary manganese levels enhance *S. aureus* virulence and infection of the murine heart. The host protein calprotectin does not limit manganese bioavailability in the heart, permitting *S. aureus* to acquire excess manganese from the diet and resist reactive oxygen species during infection.

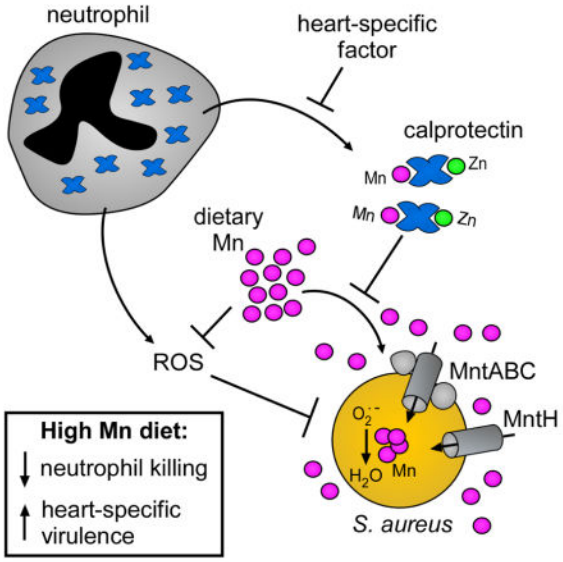

Introduction

During infection, pathogens obtain essential nutrient metals from the host (Hood and Skaar, 2012; Palmer and Skaar, 2016; Weinberg, 2009). Alterations in metal homeostasis, including increased dietary iron (Fe) and decreased dietary zinc (Zn), are associated with increased infectious disease risk (Jonker and Boele van Hensbroek, 2014; Katona and Katona-Apte, 2008). However, the current understanding of how dietary metals influence the host-pathogen relationship remains limited. Mn is a common dietary supplement, and tissue levels of Mn vary based on exposure (Greger, 1998). Furthermore, Mn is required by many bacterial pathogens for virulence (Juttukonda and Skaar, 2015). For instance, bacterial Mn import systems are required for fitness in multiple animal models of infection (Kelliher and Kehl-Fie, 2016), and some Mn-dependent enzymes are required for full virulence (Juttukonda and Skaar, 2015). Despite the importance of Mn to bacterial fitness during

infection, and the known variation in host Mn levels, the impact of dietary Mn levels on infection outcomes remains unclear.

Staphylococcus aureus is the leading cause of bacterial endocarditis (Klein and Wang, 2016) and the second most frequent agent of bloodstream infections (Anderson et al., 2014). During infection, *S. aureus* must acquire Mn for full virulence. *S. aureus* encodes two Mn acquisition systems, *mntH* and *mntABC* (Horsburgh et al., 2002a), and genetic inactivation of both Mn transporters impairs *S. aureus* infection of the liver and the kidney (Kehl-Fie et al., 2013). *S. aureus* also encodes two superoxide dismutase enzymes, *sodA* and *sodM*, that are important for surviving neutrophil-mediated killing and colonizing the liver (Kehl-Fie et al., 2011). SodA is a strict Mn-requiring enzyme and SodM can utilize Mn or Fe (Garcia et al., 2017), underscoring the importance of Mn for *S. aureus* pathogenesis. Intriguingly, several risk factors for *S. aureus* infection, including intravenous drug use and liver disease, can increase tissue Mn levels by up to 20-fold (Btaiche et al., 2011, Sikk et al., 2013). However, the impact of dietary Mn on *S. aureus* infection is unknown.

The host possesses mechanisms to restrict essential metals from microbes during infection, collectively termed ‘nutritional immunity’ (Hood and Skaar, 2012; Weinberg, 1975). Nutritional immunity encompasses an array of small molecule and protein metal chelators and metal transporters that combine to minimize metal availability as part of the inflammatory response. However, nutritional immunity can be overwhelmed by dietary metal intake. Dietary Fe supplementation enhances *Mycobacterium avium* infection in mice (Dhople et al., 1996), and excess dietary Zn allows *Clostridium difficile* to overcome host Zn sequestration (Zackular et al., 2016). These studies suggest that nutritional immunity is limited in its capacity to sequester dietary metals, and excess dietary Mn may affect the outcome of infection.

The only known Mn sequestering protein in vertebrates is calprotectin, a heterodimer of the S100 family proteins S100A8 and S100A9 (MRP8/14). Calprotectin constitutes the majority of the cytoplasmic protein pool of the neutrophil and is also expressed by other cells that respond to inflammatory signals, such as epithelial cells (Frosch et al., 2005). Chelation of the divalent cations Mn (II), Zn (II), and Fe (II) by calprotectin inhibits bacterial growth *in vitro* (reviewed in Palmer and Skaar, 2016), and calprotectin-deficient mice exhibit altered sensitivity to multiple bacterial pathogens (reviewed in Juttukonda and Skaar, 2015). In the liver, calprotectin competes with bacterial Mn and Zn importers for access to Mn and Zn, demonstrating that calprotectin restricts bacterial access to metals in this tissue during infection (Hood et al., 2012; Kehl-Fie et al., 2013; Juttukonda et al., 2016). Consistent with this, calprotectin-deficient mice systemically infected with *S. aureus* have increased Mn levels in liver lesions (Corbin et al., 2008). However, calprotectin-deficiency does not significantly impact the fitness of *Salmonella* strains lacking Mn import systems in a gastrointestinal infection model (Diaz-Ochoa et al., 2016), suggesting that calprotectin-dependent Mn sequestration may be restricted to certain tissues.

Here we set out to investigate the contribution of dietary Mn to murine Mn homeostasis, to determine how alterations in dietary Mn levels impact the outcome of systemic *S. aureus* infection, and to define the ability of calprotectin-mediated nutritional immunity to limit the

impact of high Mn diet on infection. We show that high dietary Mn elevates Mn levels in the heart and calprotectin does not restrict *S. aureus* access to Mn in this organ. Excess dietary Mn enhances *S. aureus* growth and virulence in the heart by protecting *S. aureus* from reactive oxygen species and neutrophil killing. These results suggest that host Mn sequestration is limited in the heart and demonstrate that excess dietary Mn favors *S. aureus* in the host-pathogen battle for this essential nutrient.

Results

Dietary Mn alters tissue levels

To interrogate the impact of dietary Mn on systemic *S. aureus* infection, C57BL/6 (WT) mice were fed custom-synthesized diets containing the minimum recommended concentration of Mn (Control: 10 ppm), no Mn (Low Mn: 0 ppm), or excess Mn (High Mn: 500 ppm; standard mouse chow contains 160 ppm [LabDiet® 5K52]). Mice fed each of the diets exhibited no differences in weight gain, food consumption, or histopathology in hearts, livers, kidneys, or the gastrointestinal tract (Supplementary Figure 1A–C and data not shown).

We next assessed the impact of dietary Mn on tissue Mn levels. Mn concentrations were measured in heart and liver homogenates by inductively coupled plasma mass spectrometry (ICP-MS). Organs from mice provided a high Mn diet harbored significantly higher Mn levels compared to organs from mice fed control diet, while other metals were unchanged (Figure 1A–B & Supplementary Figure 1D–J). Mice fed low Mn diet also exhibited lower Mn levels than mice fed control diet in the heart (Figure 1A). From this, we conclude that tissue Mn levels are altered by dietary Mn intake.

High dietary Mn promotes *S. aureus* infection of the heart

To test the hypothesis that Mn levels in infected tissues could alter *S. aureus* infection, we infected mice fed high Mn, control, or low Mn diet. Following intravenous challenge with *S. aureus,* mice provided a high Mn diet displayed significantly increased mortality (Figure 1C), with 80% survival of mice fed control diet but less than 20% survival of mice fed high Mn diet. Mice fed high Mn diet also exhibited ten-fold higher bacterial burdens in the heart (Figure 1D) and significantly more staphylococcal abscesses in the heart (Figure 1E & F). High Mn diet did not alter bacterial burdens in the kidney or the liver (Figure 1G & H). Interestingly, feeding mice a low Mn diet resulted in a reduction in bacterial burdens in the liver (Figure 1I), suggesting that Mn levels in the control diet but not the low Mn diet support staphylococcal growth in the liver. To determine whether other dietary metals promote *S. aureus* virulence in the heart, mice were fed diets containing altered levels of zinc (Control: 29 ppm; High Zn: 1000 ppm; Low Zn: 0 ppm) and infected with *S. aureus.* Heart bacterial burdens were unchanged by the level of dietary Zn (Figure 1J). Finally, we assessed the impact of dietary Mn on the recruitment of neutrophils, which are a critical effector cell for controlling *S. aureus* infection (Rigby and DeLeo, 2012). Phagocyte recruitment to infected hearts was unchanged by providing mice a high Mn diet (Figure 1K & L). Together, these results demonstrate that excess dietary Mn enhances *S. aureus* virulence and promotes growth of *S. aureus* in the heart but not in the kidney or the liver.

Dietary Mn does not drastically alter the gut microbiota or other bacterial infections

We next interrogated whether dietary Mn indiscriminately enhances microbial fitness within the host. Providing mice with low or high Mn diets did not significantly alter the structure or diversity of the gut microbiota (Figure 2A–C). Furthermore, mice that were placed on high or low Mn diet did not exhibit differential pathology following oral challenge with the gastrointestinal pathogen *Clostridium difficile* (Figure 2D). Finally, *Acinetobacter baumannii* fitness in both pneumonia and systemic murine infection models was not affected by dietary Mn level (Figure 2E–G). Together, these findings demonstrate that not all microbes have altered fitness in a host fed excess Mn.

Calprotectin promotes *S. aureus* infection of the heart

Essential metals are withheld from invading pathogens by a metal-sequestration response, collectively termed ‘nutritional immunity’ (Hood and Skaar, 2012; Palmer and Skaar, 2016; Weinberg, 1975). Because excess dietary Mn enhances *S. aureus* growth in the heart, we hypothesized that the host does not effectively sequester Mn in this organ. Calprotectin, a heterodimer formed by S100A8 and S100A9, is the only known Mn-sequestering immune protein in vertebrates (Corbin et al., 2008). In the livers of mice, calprotectin sequesters Mn (Corbin et al., 2008; Kehl-Fie et al., 2013), and *S100a9*$^{-/-}$ mice, which are calprotectin-deficient, exhibit higher bacterial burdens in the liver (Corbin et al., 2008). We determined that calprotectin was recruited to *S. aureus*-infected hearts when mice were provided high Mn diet, but calprotectin was not detected in mock-infected mice or *S100a9*$^{-/-}$ infected mice (Figure 3A). Of note, calprotectin was present surrounding the staphylococcal abscess but not in the abscess center (Supplementary Figure 2A–C), which contrasts with previous findings in the liver (Corbin et al., 2008) and the kidney (Kehl-Fie et al., 2013), where calprotectin is found throughoutth the staphylococcal abscess. Interestingly, significantly fewer bacteria were recovered from the hearts of *S100a9*$^{-/-}$ mice than WT mice for each diet (Figure 3B), with a 6-$\log_{10}$ reduction in bacterial burdens in *S100a9*$^{-/-}$ mice fed a low Mn diet. Moreover, *S100a9*$^{-/-}$ mice were protected from infection mortality when fed high Mn diet (Figure 3C). These findings demonstrate that calprotectin is present in infected hearts and supports bacterial growth in this organ.

Calprotectin does not restrict Mn availability in the heart

S. aureus possesses two Mn importers, MntH and MntABC (Kehl-Fie et al., 2013). *S. aureus* inactivated for both importers (Δ*mntH/C*) displays a growth defect that can be rescued with excess Mn, showing that growth of this strain can be used as a biological readout for Mn availability (Supplementary Figure 3A). Similar to other high-affinity metal transporters, MntH and MntABC are not required if Mn is abundant (Moore and Helmann, 2005), likely because promiscuous transporters deliver Mn across the membrane. To assess whether loss of calprotectin alters Mn bioavailability in the heart, mice were infected with *S. aureus* WT or Δ*mntH/C.* Heart bacterial burdens of Δ*mntH/C* were not different in WT or *S100a9*$^{-/-}$ mice (Figure 4A), indicating that loss of calprotectin does not affect Mn bioavailability in the heart. In contrast, Δ*mntH/C* colonizes to higher bacterial burdens in the livers of *S100a9*$^{-/-}$ mice compared to WT mice (Kehl-Fie et al., 2013). Similarly, another strain sensitive to Mn-limitation, Δ*sodA/M,* was not rescued in the hearts of *S100a9−/−* mice

(Supplementary Figure 3B). These findings suggest that calprotectin does not sequester Mn in the heart.

Since calprotectin-deficient mice have lower bacterial burdens than WT mice when fed low Mn diet, we postulated that calprotectin may have a role in delivering Mn to the heart. However, the absence of calprotectin had little impact on Mn levels in *S. aureus* infected hearts, kidneys or livers (Figure 4B, Supplementary Figure 3C & D). These results demonstrate that calprotectin is not important for maintaining total Mn levels in the heart, liver, or kidney during infection.

We considered the possibility that Mn-bound calprotectin serves as a nutrient source for *S. aureus,* as calprotectin supports staphylococcal growth in the heart. *Neisseria* species scavenge Zn from calprotectin *in vitro,* a process termed 'zinc piracy' (Jean et al., 2016; Stork et al., 2013). We assessed whether *S. aureus* can utilize calprotectin as a source for nutrient Mn by disc diffusion assay. *S. aureus* plated at low density was unable to grow utilizing Mn-loaded calprotectin as a metal source, whereas excess free $MnCl_2$ supported growth (Figure 4C). When *S. aureus* was plated at a high density, apo calprotectin inhibited growth of *S. aureus* but Mn-loaded calprotectin did not, indicating that the metal-binding sites were saturated (Figure 4C). Similarly, calprotectin that lacks the Mn and Zn binding sites (ΔS1/ΔS2) (Kehl-Fie et al., 2011) did not inhibit growth (Figure 4C). Based on these findings, we conclude that *S. aureus* does not possess mechanisms to scavenge Mn from calprotectin. Taken as a whole, these data suggest that calprotectin does not play a major role in Mn nutritional immunity during *S. aureus* infection of the heart.

Calprotectin promotes neutrophil accumulation to support staphylococcal infection

We sought to understand why *S100a9*$^{-/-}$ mice have lower bacterial burdens than WT mice in the heart. Calprotectin-deficient mice are protected from intraperitoneal infection with *S. aureus* due to decreased secretion of pro-inflammatory cytokines (Cho et al., 2015; Vogl et al., 2007). However, there were no differences in IL-1β, IL-6, IL-17, or TNFα in heart tissue of WT and *S100a9*$^{-/-}$ mice (Supplementary Figure 3 E–H). To discern at which stage of infection protection occurs, a timecourse experiment was performed. Bacterial burdens of WT and *S100a9*$^{-/-}$ mice are similar at 2 and 6 hours post infection, but *S100a9*$^{-/-}$ mice have lower bacterial numbers by 24 hours post infection (Figure 5A). These results suggest that WT mice permit bacterial replication within the heart whereas *S100a9*$^{-/-}$ mice clear *S. aureus* from the heart. Staphylococci contained within abscess lesions are not typically cleared by the host (Cheng et al., 2009). Therefore, we hypothesized that abscess formation is disrupted in *S100a9*$^{-/-}$ mice, permitting bacterial clearance. Gross and histopathological analyses of infected cardiac tissue from WT and *S100a9*$^{-/-}$ mice revealed that *S100a9*$^{-/-}$ hearts lack the well-formed abscess lesions present in WT hearts (Figure 5B & C). Consistent with the decreased inflammation observed in histopathologic sections, *S100a9*$^{-/-}$ mice have fewer cardiac neutrophils ($Ly6G^+$ $CD11b^{hi}$) four days post infection than WT mice (Figure 5D), but no differences in macrophages (Supplementary igure 3I). Thus, calprotectin promotes neutrophil accumulation in *S. aureus*-infected hearts.

To test the hypothesis that neutrophils are required for the differential bacterial burdens between *S100a9*$^{-/-}$ and WT mice, neutrophils were depleted by treatment with an anti-Ly6G

antibody and bacterial burdens were assessed. Consistent with our hypothesis, bacterial burdens were the same when both *S100a9*$^{-/-}$ and WT mice were depleted of neutrophils, whereas *S100a9*$^{-/-}$ mice exhibited decreased bacterial burdens when treated with the isotype control antibody (Figure 5E). Furthermore, transplanting *S100a9*$^{-/-}$ mice with WT bone marrow was sufficient to increase bacterial burdens in the heart (Figure 5F). From these data, we conclude that calprotectin expression by hematopoietic stem cells alters neutrophil behavior in a manner that promotes infection.

Calprotectin is a known ligand for the membrane-embedded toll-like receptor 4, encoded by *Tlr-4*, and the receptor for advanced glycation end products, encoded by *Ager* (Vogl et al., 2007; Yan et al., 2013). We considered the possibility that secreted calprotectin could ligate these receptors to promote inflammation and infection. However, neither *Tlr-4*$^{-/-}$ nor *Ager*$^{-/-}$ mice had decreased bacterial burdens relative to WT mice (Figure 5G & H), indicating that these receptors likely do not promote staphylococcal infection of the heart. To discern whether calprotectin alters neutrophil behavior in a cell-intrinsic manner, bone marrow transplants were performed with a 1:1 mixture of WT and *S100a9*$^{-/-}$ bone marrow (Supplementary Figure 4A). Following *S. aureus* infection, nearly twice as many WT neutrophils were present in infected hearts relative to *S100a9*$^{-/-}$ neutrophils (Figure 5I, Supplementary Figure 4B & C). This result indicates that calprotectin promotes neutrophil accumulation at the site of infection in a cell-intrinsic manner. CD11b level was the same between WT and *S100a9*$^{-/-}$ neutrophils (Figure 5J), demonstrating that migration differences were not due to upregulation of β_2-integrins, such as CD11b, in WT mice (Ryckman et al., 2003). Consistent with the defect in neutrophil recruitment being cell-intrinsic, few *S100a9*$^{-/-}$ neutrophils were recruited to infected hearts when transplanted into WT mice, while WT neutrophils were robustly recruited to infected hearts when transplanted into *S100a9*$^{-/-}$ mice (Supplementary Figure 4D & E). Moreover, *S100a9*$^{-/-}$ bone marrow transplanted into WT mice decreased bacterial burdens in the heart (Figure 5K). Taken as a whole, these data demonstrate that calprotectin regulates neutrophil recruitment and abscess formation within the heart and suggest that *S. aureus* replicates more robustly within heart abscess lesions.

Excess dietary Mn is bioavailable to *S. aureus* in the heart

The finding that calprotectin deficiency does not alter Mn bioavailability in the heart suggests that the host may have a limited ability to sequester excess Mn in this tissue. To determine if excess Mn in the heart is in proximity to staphylococcal abscesses and available for bacterial capture, the spatial localization of Mn was examined using laser ablation coupled to ICP-MS (LA-ICP-MS). Uninfected hearts displayed relatively homogeneous Mn and calcium (Ca) concentrations throughout the myocardium (Figure 6A). When mice were provided control diet, Mn was depleted in the staphylococcal abscess relative to the adjacent myocardium (Figure 6B), similar to the Mn-deplete staphylococcal abscesses observed in livers and kidneys (Corbin et al., 2008; Kehl-Fie et al., 2013). In contrast, mice fed high Mn diet displayed high concentrations of Mn surrounding the staphylococcal abscesses (Figure 6B). Ca accumulated within abscesses of mice on both control and high Mn diet (Figure 6B). Similar LA-ICP-MS results were obtained in calprotectin-deficient mice (Supplementary Figure 2C). These findings suggest that excess dietary Mn may accumulate

in the heart in a location available for acquisition by *S. aureus.* To test this hypothesis, mice were infected with *S. aureus* WT or Δ*mntH/C,* which serves as a readout for Mn bioavailability. When mice were fed control diet, 6-$\log_{10}$ fewer CFUs were recovered from Δ*mntH/C* infection than WT infection (Figure 6C), implying that hearts are Mn deplete at baseline. However, the fitness deficit for Δ*mntH/C* was significantly and profoundly reversed in mice fed high Mn diet (Figure 6C). These results indicate that excess dietary Mn is bioavailable to *S. aureus* in the heart.

Dietary manganese protects *S. aureus* from superoxide stress

We hypothesized that high Mn diet may protect *S. aureus* from reactive oxygen species (ROS) produced during the host immune response. Mn has multi-faceted roles in bacterial defense against ROS (Horsburgh et al., 2002b; Lisher and Giedroc, 2013). Neutrophils, which are essential for clearance of *S. aureus,* are capable of killing *S. aureus* through the production of ROS (Rigby and DeLeo, 2012). Therefore, we posited that *S. aureus* may utilize the increase in bioavailable Mn to detoxify ROS and escape neutrophil-mediated killing.

S. aureus expresses superoxide dismutase enzymes, SodA and SodM, which can use Mn to detoxify superoxide (Garcia et al., 2017; Kehl-Fie et al., 2011). SodA and SodM confer resistance to neutrophil killing, and staphylococcal SOD activity is impaired by Mn-chelation (Kehl-Fie et al., 2011). To assess the contribution of SOD to infection of the heart, mice fed control and high Mn diet were infected with WT *S. aureus* and Δ*sodA/M*. While *S. aureus* Δ*sodA/M* was attenuated approximately 5-$\log_{10}$ in mice fed control diet, Δ*sodA/M* had no fitness defect in mice fed the high Mn diet, similar to the rescue seen in neutrophil-depleted mice (Figure 7A & B). When fed a high Mn diet, mice depleted of neutrophils and infected with Δ*sodA/M* succumbed to infection (Supplementary Figure 5A). *S. aureus* SOD enzymes are therefore dispensable in the setting of excess dietary Mn, suggesting that molecular Mn detoxifies ROS independent of SOD (Lisher and Giedroc, 2013). To test this hypothesis, *S. aureus* was grown in the presence of the superoxide donor paraquat with or without added Mn (Figure 7C & Supplementary Figure 5B). As previously published (Kehl-Fie et al., 2011), Δ*sodA/M* was highly susceptible to superoxide stress. However, the addition of Mn to the medium significantly improved the growth of Δ*sodA/M* in paraquat. In fact, the rescue of WT and Δ*sodA/M* in paraquat by Mn *in vitro* mirrored the bacterial burdens recovered from hearts of mice on control or high Mn diet (Figure 7A). Hence, we propose that Mn serves as an antioxidant independent of superoxide dismutase. We confirmed that Mn protects human-derived *S. aureus* isolates from superoxide stress. To this end, methicillin-resistant and methicillin-sensitive *S. aureus* isolates from human endocarditis cases were assayed for Mn rescue of growth in paraquat (Figure 7D & Supplementary Figure 5C–E). Mn rescued all *S. aureus* isolates from superoxide growth inhibition. Interestingly, *A. baumannii* growth in paraquat was not enhanced by additional Mn, consistent with the lack of enhanced infection by *A. baumannii* in mice fed high Mn diet (Supplementary Figure 5F & G, Figure 2).

Finally, the ability of Mn to modulate human neutrophil antimicrobial activity was interrogated. Mn protected *S. aureus* from killing by human neutrophils *ex vivo*, but no

protection occurred in neutrophils treated with the NADPH oxidase inhibitor apocynin (Figure 7E). Mn did not alter bacterial growth in the absence of neutrophils or alter bacterial phagocytosis (Supplementary Figure 6A–D). Mn decreased measurements of extracellular ROS produced by neutrophils (Supplementary Figure 6E), while intracellular ROS measurements within neutrophils were enhanced by Mn (Supplementary Figure 6F). Taken together, these results suggest that dietary Mn serves as an antioxidant in the heart, protecting *S. aureus* from ROS-dependent killing by neutrophils. Therefore, modulation of a single dietary element can effectively inactivate one of the most potent activities of the vertebrate innate immune system.

Discussion

We report here that excess dietary Mn enhances *S. aureus* virulence and infection of the heart. Altering Mn concentrations in the diet results in significant changes in Mn homeostasis within hearts. Moreover, excess dietary Mn is bioavailable to *S. aureus*. Treatment with excess Mn *in vitro* protects *S. aureus* from superoxide stress and neutrophil killing, and *S. aureus* inactivated for superoxide dismutase exhibits a virulence defect in the heart that can be fully complemented by excess dietary Mn. We further report that host calprotectin deficiency does not alter Mn bioavailability or increase fitness of *S. aureus* in the heart, even in the setting of dietary Mn manipulation. In sum, these results indicate that excess dietary Mn is bioavailable to *S. aureus* in the heart and is utilized by *S. aureus* to escape neutrophil killing (Supplementary Figure 7).

We propose that calprotectin-mediated Mn sequestration is tissue specific, and that the limited ability of calprotectin to sequester Mn in the heart contributes to the heart-specific impact of dietary Mn. Calprotectin has a well-studied role in antimicrobial metal chelation *in vitro* (Kelliher and Kehl-Fie, 2016). Calprotectin decreases the abundance of Mn specifically within staphylococcal liver lesions, and Mn is bioavailable to *S. aureus* in *S100a9*$^{-/-}$ mice in the liver (Corbin et al., 2008). In the heart, we found no evidence that calprotectin sequesters Mn during *S. aureus* infection. In line with a model of tissue-specific Mn sequestration by calprotectin, staphylococcal kidney lesions are devoid of Mn even in *S100a9*$^{-/-}$ mice (Kehl-Fie et al,. 2013), and calprotectin does not impact Mn bioavailability to *Salmonella* during gastrointestinal infection (Diaz-Ochoa et al., 2016). These findings raise the possibility that additional mechanisms exist to regulate the metal-sequestering properties of antimicrobial proteins in a tissue- or context- dependent fashion.

Calprotectin may be unable to sequester Mn in the heart as a result of tissue localization. In heart lesions, calprotectin co-localizes predominantly with intact immune cells but not with zones of necrosis or staphylococcal microcolonies. This contrasts with histone H2 localization throughout much of the abscess (Supplementary Figure 3A & B). Histones are a component of neutrophil extracellular traps (Brinkmann and Zychlinsky, 2007). These results suggest that calprotectin is not released by neutrophils in the heart, a result worthy of continued investigation. Remaining confined within the neutrophil cytoplasm would exclude calprotectin from extracellular Mn chelation.

Calprotectin upregulates the expression of *S. aureus* SaeRS-regulated virulence genes in an intraperitoneal model of *S. aureus* infection (Cho et al., 2015). In the intraperitoneal model, mortality of WT mice is greater than *S100a9*$^{-/-}$ mice due to elevations in pro-inflammatory cytokines, including TNFα (Cho et al., 2015). Whether calprotectin alters expression of the SaeR regulon in the heart is unknown. However, pro-inflammatory cytokines including TNFα were not increased in WT mice in our intravenous infection model, suggesting that a different mechanism is responsible for the protection of *S100a9*$^{-/-}$ mice in the heart.

Our data suggest that calprotectin-mediated host defenses are a liability in the heart by promoting neutrophil accumulation. Notably, neutrophils are important for controlling *S. aureus* replication, as neutrophil depletion increases bacterial burdens. We propose a three-tiered model of the impact of neutrophil accumulation on *S. aureus* infection. In the absence of neutrophils, bacterial replication is unchecked. Moderate neutrophil accumulation without abscess formation, as seen in *S100a9*$^{-/-}$ mice, permits antibacterial activity with minimal host damage. Finally, excessive neutrophil accumulation and abscess formation in the heart enhances staphylococcal growth. Calprotectin stimulates neutrophil migration *ex vivo* in a TLR-4 dependent mechanism (Pruenster et al., 2015). However, deficiency in *Tlr-4* does not protect from *S. aureus* infection of the heart, and we observed that differences in accumulation were not due to an extracellular factor. Thus, the cell-intrinsic deficit in *S100a9*$^{-/-}$ neutrophil migration is not due to previously studied mechanisms. The finding that heightened neutrophil accumulation in the heart does not improve host defense against *S. aureus*, and instead promotes bacterial proliferation in this organ, is consistent with the fact that this crucial organ cannot tolerate excessive inflammation and remain functional (Mann, 2002).

We propose that baseline differences in Mn concentrations contribute to the phenotypic differences observed between the heart and the liver. In our murine model, Mn concentrations are higher in liver homogenates than heart homogenates, and similar results have been reported for human tissue (Rahil-Khazen et al., 2002). Moreover, *S. aureus* Δ*mntH/C*, which is impaired for growth when Mn is limited, is more highly attenuated in the heart (~6 $\log_{10}$) than in the liver (<1 $\log_{10}$) (Kehl-Fie et al., 2013). Similarly, *S. aureus* Δ*arlRS,* a strain lacking the ability to modulate metabolism in response to Mn starvation, is highly attenuated in the hearts of WT mice (Radin et al., 2016). These results suggest that the liver has more available Mn than the heart. Interestingly, high Mn diet did not alter bacterial burdens in the liver, despite the liver Mn increasing from ~150 ng/g to ~600 ng/g. High Mn diet did increase bacterial burdens in the heart, where Mn levels increased from ~60 ng/g for control diet to ~160 ng/g for high Mn diet. These results suggest that Mn has a threshold effect on bacterial growth, with concentrations in homogenates around 100 ng/g sufficient for full virulence. Consistent with this hypothesis, feeding mice a low Mn diet decreased Mn levels in the liver to ~80 ng/g and also resulted in decreased bacterial burdens.

We found that *S. aureus* can counteract ROS and neutrophil killing through a Mn-dependent mechanism. However, high Mn diet enhances staphylococcal virulence through a neutrophil-independent mechanism as well, as neutrophil-depleted mice fed high Mn diet succumbed to *S. aureus* Δ*sodA/M* infection but neutrophil-depleted mice fed control diet did not. Mn has been reported to serve as an antioxidant through several mechanisms, including serving as a

cofactor for SOD enzymes, substituting for Fe in mononuclear enzymes to protect from hydrogen peroxide stress, and by scavenging superoxide via small molecular weight complexes (Lisher and Giedroc, 2013). The finding that *S. aureus* Δ*sodA/M* is rescued by Mn in culture suggests that low molecular weight complexes of Mn and phosphate and/or carbonate contribute significantly to superoxide detoxification (Barnese et al., 2012). Importantly, Δ*sodA/M* rescue by high Mn diet in the heart provides evidence that these low molecular weight Mn complexes serve as an antioxidant during infection. This provides significant relevance for future studies into the importance of Mn low molecular weight complexes during infection.

This work provides proof-of-principle that excess dietary Mn can alter *S. aureus* virulence by protecting invading organisms from the host immune response. The clinical relevance of this finding remains to be assessed. *S. aureus* is the leading cause of bacterial endocarditis (Klein and Wang, 2016) and the second leading cause of bloodstream infections worldwide (Anderson et al., 2014). Notably, there are shared risk factors for the development of these infections and increased Mn levels. A significant risk factor for *S. aureus* endocarditis is intravenous drug use (Tong et al., 2015), even comparing amongst a cohort of individuals with *S. aureus* bacteremia (Le Moing et al., 2015). Intriguingly, IV drug users can exhibit up to a 20-fold increase in Mn levels in hair (Sikk et al., 2013). In addition, intravenous catheters are a significant risk factor for *S. aureus* bacteremia and endocarditis (Tong et al., 2015); serum levels of Mn are 2–4 times higher in people on long-term intravenous diets (Btaiche et al., 2011). Finally, chronic liver disease is a risk factor for *S. aureus* endocarditis, and impaired Mn excretion caused by liver disease can drastically elevate Mn levels (Hauser et al., 1994; Hung et al., 2013). Potential links between Mn levels and infection susceptibility or severity warrant further study in clinical trials. Limiting Mn exposure, such as by avoiding nutritional supplements that contain high amounts of Mn, may be an avenue to decrease risk of *S. aureus* infection.

STAR Methods

CONTACT FOR REAGENT AND RESOURCE SHARING

Further information and requests for resources and reagents should be directed to and will be fulfilled by the Lead Contact, Eric Skaar (eric.skaar@vanderbilt.edu).

EXPERIMENTAL MODEL AND SUBJECT DETAILS

Ethics Statement—All animal experiments were reviewed and approved by the Institutional Animal Care and Use Committee of Vanderbilt University and performed according to NIH guidelines, the Animal Welfare Act, and US Federal law. *S. aureus* clinical isolates were obtained under a protocol approved by the Vanderbilt Institutional Review Board. Blood was obtained from healthy, de-identified, consenting adult donors as buffy coats from the New York Blood Center. Fresh human serum was prepared by drawing blood from consented healthy volunteers under a New York University Institutional Review Board approved protocol (NYU IRB protocol i14-02129).

Animals—C57BL/6, CD45.1 (Ly5.1)-congenic, and *Tlr-4*$^{-/-}$ mice were purchased from The Jackson Laboratory. *S100a9*$^{-/-}$ and *Ager*$^{-/-}$ mice (on a C57BL/6 background) were maintained in our animal colony. Females were used for all experiments except *C. difficile* infections, and all mice were between 9 and 14 weeks of age at the time of infection. Specifically, mice fed custom-synthesized diets were 12–14 weeks old at the time of infection. Mice in Figure 4A and Supplementary Figure 3B were 8–9 weeks old at the time of infection and fed normal chow prior to infection. *C. difficile* infection studies were conducted on adult (8 to 12 week old) age-matched male C57BL/6 mice. Typical weight and food intake data is included in Supplementary Figure 1A & B. Mice were housed, 5 to a cage, in specific pathogen free conditions. Food and water was provided ad libitum. Mice were assigned to experimental groups using a random number generator. All animal experiments were approved and performed in compliance with the Vanderbilt Institutional Animal Care and Use Committee (IACUC).

Bacterial strains—Experiments utilized the *S. aureus* strain Newman and derivatives, including Δ*mntH/C* (Kehl-Fie et al., 2013) and Δ*sodA/M* (Kehl-Fie et al., 2011), unless otherwise noted. Clinical isolates of *S. aureus* were provided by the VUMC Clinical Microbiology Laboratory from blood and/or valve cultures of diagnosed cases of bacterial endocarditis; these isolates were identified by multiple FDA-approved phenotypic methodologies. *A. baumannii* strain ATCC 17978 was utilized for infections and growth curves as noted. *S. aureus* and *A. baumannii* stocks were maintained as −80°C stocks and streaked 2 days prior to each experiment. *S. aureus* and *A. baumannii* liquid cultures were grown at 37°C with 180 rpm shaking. Tryptic soy broth (TSB) was utilized as growth medium for *S. aureus* and solid medium contained 2% agar. Luria broth (LB) was utilized as growth medium for *A. baumannii* and solid medium contained 2% agar. *C. difficile* strain 630 was utilized for the gastrointestinal *C. difficile* infection. *C. difficile* was cultured on taurocholate cycloserine cefoxitin fructose agar (TCCFA) at 37°C in an anaerobic chamber (Coy, Grass Lake, MI).

Human neutrophils—Human neutrophils (hPMN) were isolated from buffy coats from anonymous, healthy donors (New York Blood Center) as previously described (Reyes-Robles et al., 2016). No information about the donors, including sex, is known. In short, hPMNs were separated from erythrocytes with 3% dextran (Dextran 500; Pharmacosmos) in 0.9% sodium chloride (Baxter). The hPMNs were subsequently separated from peripheral blood mononuclear cells (PBMCs) by a Ficoll gradient (Ficoll-Paque PLUS; GE). Remaining erythrocytes were lysed by using ACK lysing buffer (Gibco).

METHOD DETAILS

Dietary Manipulation—Diets were synthesized by Dyets Inc. (Bethlehem, PA) using the AIN-93M standardized diet (Reeves et al., 1993). The base diet was formulated as a Mn and Zn-free diet, with Mn and Zn added as carbonate salts to the following specified concentrations: control: 10 ppm Mn, 29 ppm Zn; low Mn: 0 ppm Mn, 29 ppm Zn; high Mn: 500 ppm Mn, 29 ppm Zn; low Zn: 10 ppm Mn, 0 ppm Zn; high Zn: 10 ppm Mn, 1000 ppm Zn. Six-week old female mice were placed on custom-synthesized diets for 6–8 weeks prior

to infection and throughout infection, except for the *C. difficile* study which utilized male mice.

***S. aureus* growth curves—**Bacterial strains were freshly streaked onto TSA two days prior to growth curves. Overnight cultures were grown in 5 mL of TSB overnight until the cultures reached stationary phase. These overnight cultures were subsequently diluted 1/100 into 96-well round-bottom plates containing tryptic soy broth (BD, Franklin Lakes NJ) with or without 1 mM or 5 mM paraquat (Sigma, St. Louis MO) and 1 mM $MnCl_2$, as indicated in the figure legend. The 96-well plates were incubated at 37°C with shaking. Growth was monitored by absorbance at OD_{600} every hour utilizing a plate reader (BioTek, Winooski VT). Bacterial growth curves were repeated three times. Each experiment utilized biological triplicate cultures.

***A. baumannii* growth curves—**Bacterial strains were freshly streaked onto LBA two days prior to growth curves. Overnight cultures were grown in 3 mL of LB overnight until the cultures reached stationary phase. These overnight cultures were subsequently diluted 1/100 into 96-well round-bottom plates containing tryptic soy broth (BD, Franklin Lakes NJ) with or without 500 μM paraquat (Sigma, St. Louis MO) and 500 μM, 250 μM, or 125 μM $MnCl_2$, as indicated in the figure legend. Concentrations of Mn above 500 μM inhibited *A. baumannii* growth. 96-well plates were incubated at 37°C with slow orbital shaking in an Epoch 2 plate reader (BioTek, Winooski VT), and growth was monitored by absorbance at OD_{600} every 30 minutes. Growth curves were repeated three times. Each experiment utilized biological triplicate cultures.

Murine model of *S. aureus* systemic infection—Mice were inoculated by intravenous injection of the retroorbital sinus with *S. aureus* grown to mid-exponential phase, washed, and resuspended in 100 μL ice-cold PBS. Specifically, *S. aureus* WT and derivatives were freshly streaked from frozen stocks onto TSA two days prior to infection. Overnight cultures were grown in TSB for 15 hours then sub-cultured 1:100 into 5 mL of TSB. Mid-exponential phase cultures were harvested by centrifugation, washed in PBS, and resuspended in PBS for infection. The inoculum utilized was 2×10^7 CFU unless otherwise noted. Survival experiments utilized an inoculum of 5×10^7 CFU. An inoculum of 1×10^7 CFU was used for mice considered to potentially have high susceptibility, such as neutrophil-depleted mice. Specifically, the inoculum of 1×10^7 CFU was used for Figure 4A, Supplemental Figure 3B, Figure 5E & F, and Figure 5I–K. Mice were anesthetized with intraperitoneal injection of 2,2,2-tribromoethanol diluted in PBS. Mice were monitored prior to humane euthanasia by inhalation of CO_2. Infections were carried out for four days unless otherwise noted. The infection was 18 hours for Figure 1K & L, 24 hours for Supplementary Figure 3 E–H, and various timepoints as indicated for Figure 5A. Livers, hearts, spleens, lungs and kidneys were removed and processed as indicated in the figure legends. To determine bacterial load, organs were homogenized in sterile PBS and serial dilutions were spot-plated onto TSA. For imaging mass spectrometry analyses, organs were flash-frozen in liquid nitrogen and stored at −80°C. For histopathological analysis, organs were fixed in 10% formalin, paraffin-embedded and sectioned.

Murine model of *C. difficile* infection—Mice were subjected to a previously described model of *C. difficile* infection (Zackular et al., 2016). Briefly, mice were given cefoperazone in their drinking water (0.5 mg/ml) for five days. Mice were then given two days of recovery prior to administration of 10^5 spores of *C. difficile* strain 630 in PBS via oral gavage. Prior to infection, each mouse was confirmed to be *C. difficile* culture negative. Following infection mice were monitored for signs of severe disease, including inappetence, diarrhea, hunching, and weight loss. Mice that exhibited severe disease or weight loss in excess of 20% were humanely euthanized. All animal experiments were approved and performed in compliance with the Institutional Animal Care and Use Committee (IACUC). At necropsy, ceca and colons were harvested, fixed in 10% formalin solution, and embedded in paraffin. Sections were stained with hemotoxylin and eosin. Each section was given a disease score by a pathologist in a blinded fashion based on previously described criteria (Zackular et al., 2016). Specifically, histological scores were reported as a cumulative score of three independent scoring criteria: inflammation, edema, and epithelial cell damage.

***A. baumannii* pneumonia model—**A mouse pneumonia model of *A. baumannii* infection was employed as previously described (Hood et al., 2012). Briefly, *A. baumannii* ATCC 17978 was freshly streaked from frozen stocks onto LB agar two days prior to infection. Overnight cultures were grown in LB. On the day of the infection, overnight cultures were sub-cultured 1:1,000 in 10 mL of LB and grown to mid-exponential phase. Cells were then harvested by centrifugation, washed twice in PBS, and resuspended in PBS to a final concentration of 1×10^{10} CFU mL^{-1}. Mice were anesthetized with intraperitoneal injection of 2,2,2-tribromoethanol diluted in PBS. Anesthetized mice were inoculated intranasally with 3×10^8 CFU in 30 μL volume. Infection proceeded for 36 hours. Mice were then euthanized with CO_2 and lungs and livers removed and placed on ice. Organs were homogenized in 1 mL PBS, serially diluted in PBS, and dilutions were spot-plated onto LB agar. Infections were performed at the Vanderbilt University Medical Center and were approved and performed in compliance with the Institutional Animal Care and Use Committee (IACUC).

A. baumannii* systemic infection model—A. baumannii* ATCC 17978 was freshly streaked from frozen stocks onto LB agar two days prior to infection. Overnight cultures were grown in LB. On the day of the infection, overnight cultures were sub-cultured 1:1,000 in 10 mL of LB and grown to mid-exponential phase. Cells were then harvested by centrifugation, washed twice in PBS, and resuspended in PBS to a final concentration of 1×10^{10} CFU mL^{-1}. Mice were anesthetized with intraperitoneal injection of 2,2,2-tribromoethanol diluted in PBS. Anesthetized mice were inoculated intravenously with 1×10^9 CFU in a 100 μL volume. Infection proceeded for 24 hours. Mice were then euthanized with CO_2 and lungs, livers, kidneys, spleens and hearts removed and placed on ice. Organs were homogenized in sterile PBS in NAVY bullet blender tubes (Next Advance, Averill Park, NY) in a bullet blender (Next Advance, Averill Park, NY) at speed 8 for 5 minutes and speed 10 for 3 minutes. Homogenates were serially diluted in PBS, and dilutions were spot-plated onto LB agar. Infections were performed at the Vanderbilt University Medical Center and were approved and performed in compliance with the Institutional Animal Care and Use Committee (IACUC).

Neutrophil depletion—Mice were intraperitoneally injected with 250 μg anti-Ly6G monoclonal antibody, clone 1A8, or isotype control antibody, clone 2A3 (BioLegend, San Diego CA). Antibodies were diluted in sterile PBS (Corning, Corning NY) and administered 24 hours prior to infection and daily throughout infection.

Hematopoietic stem cell transplants—Recipient mice were lethally irradiated via Cesium-137 exposure (11 Grays, split dose) and adoptively transferred with 10 million donor cells. The bone marrow was reconstituted for at least seven weeks following transplant and chimerism was found to be >95% donor cells. For mixed donor transplants, a one-to-one ratio of donors was confirmed by flow cytometry analysis of CD45.1 and CD45.2.

16S rRNA sequencing and microbiota analysis—Fresh fecal samples were collected from individual mice ($N = 3$) during a four-week time-course of diet manipulation and immediately frozen for storage at −20°C. DNA was isolated from fecal samples using the PowerSoil DNA isolation kit (MO BIO Laboratories). For each sample, the V4 region of the 16S rRNA gene was amplified and sequenced using the Illumina MiSeq Personal Sequencing platform and sequences were curated using the mothur software package, as previously described (Schloss et al., 2009; Zackular et al., 2016). After curation, we obtained between 8,297 and 23,327 sequences per sample (median=13,015), with a median length of 253 bp. Sequences were clustered into operational taxonomic units (OTUs) based on a 3% distance cutoff calculated using the average-neighbor algorithm. The dataset was rarefied to 8,297 sequences per sample to limit the effects of uneven sampling. All sequences were classified using the RDP training set (version 9) and OTUs were given a consensus classification using a naïve Bayesian classifier. Microbial biodiversity (alpha-diversity) was calculated using the inverse Simpson's index, species richness was calculated using Sobs (observed OTUs), and structure (beta-diversity) was calculated using the θ_{YC} distance metric with OTU frequency data. Analysis of molecular variance (AMOVA) was performed to determine significance between the community structures of different groups of samples based on θ_{YC} distance matrices.

Tissue sectioning for imaging analysis—Hearts were sectioned at −20°C using a Thermo Fisher Scientific CryoStar NX70 Cryostat (Thermo Fisher Scientific, Waltham, MA). For MALDI IMS, hearts were sectioned at 10 μm thickness and thaw-mounted onto chilled Indium-tin-oxide float coated glass slides with a resistance of 30–60 Ω (Delta Technologies, Loveland, CO, USA). Sections for histological analysis were collected onto microscope slides, hematoxylin and eosin stained, and scanned at 20x magnification using a Leica SCN400 Brightfield Slide Scanner (Leica Microsystems, Buffalo Grove, IL, USA.) Sections for LA-ICP MS were sectioned at 30 μm thickness and thaw-mounted onto nitric-acid washed poly(L)lysine-coated vinyl slides (Electron Microscopy Sciences, Hatfield, PA.)

Protein imaging mass spectrometry—Heart sections for MALDI IMS analysis were washed to remove interfering lipids and salts similarly to previously described (Spraggins et al., 2015). Briefly, slides were subjected to sequential washes of 70% ethanol for 30 s, 100% ethanol for 30 seconds, Carnoy fluid (6:3:1 ethanol:chloroform:acetic acid) for 120 seconds,

70% ethanol for 30 seconds, and 100% ethanol for 30 seconds. 2,5-dihydroxyacetophenone (DHA) was used as a matrix and prepared to a concentration of 15 mg/mL in 90% acetonitrile with 0.1% trifluoroacetic acid. Matrix was applied to tissue sections using a TM Sprayer (HTX Technologies, Carrboro, NC). The instrument was operated at a flow rate of 0.15 ml/minute with 90% acetonitrile as a pushing solvent. Six passes of matrix were sprayed in a criss-cross pattern at a speed of 1100 mm/minute with a 2 mm spacing between sprays. The matrix coating was rehydrated immediately before analysis in a rehydration chamber (Yang and Caprioli, 2011) in a 55° oven for 3 minutes using 50 mM acetic acid. IMS was performed using a rapifleX MALDI Tissuetyper (Bruker Daltonics, Billerica, MA, USA) equipped with a Smartbeam 3D 10 kHz Nd:YAG laser (355 nm). The laser was operated in 2 mod 5 mode with a pixel scan of 40 μm in both x and y directions. Data were collected from *m/z* 2000-20,000 with 500 laser shots collected at each pixel.

Elemental imaging—Elemental imaging was performed using LSX-213 laser ablation system (*LA*, CETAC, Omaha, USA) online coupled with ELEMENT 2™ inductively coupled plasma mass spectrometry (*HR-ICPMS*, Thermo Fisher Scientific, Bremen, Germany). Slide-mounted slices of mouse heart were placed in sealed ablation cell and ablated in multi-parallel-line mode with a focused Nd:YAG laser beam at a round-shaped spot size of 100 μm diameter. The ablated sample particles were then transferred to ICP-MS for the detection under medium resolution (R=4200).

Digestion of tissues for ICP MS—Whole organs were homogenized in 1 mL PBS in Whirl Paks (Nasco, Fort Atkinson, WA) and digested in 2 mL HNO_3 and 500 μL H_2O_2 (Optima grade metal-free; Fisher, Waltham, MA) at 90 °C overnight in metal-free Teflon jars. Digested samples were then transferred to metal-free 15 mL conical tubes and diluted with 9 mL MilliQ deionized water and submitted for inductively coupled plasma mass spectrometry (ICP-MS) analysis at the Vanderbilt Mass Spectrometry Research Center.

ICP-MS—Element quantification analysis on liquid digested samples was performed using ELEMENT 2™ high resolution inductively coupled plasma mass spectrometry (*HR-ICPMS*, Thermo Fisher Scientific, Bremen, Germany) coupled with ESI auto sampler (Elemental Scientific, Omaha, NE). The ICPMS is equipped with a PFA microflow nebulizer (Elemental Scientific, Omaha, NE), a Scott double-pass spray chamber (at room temperature), a magnetic sector followed by an electric sector, and a second electron multiplier. Liquid sample was up-taken by self-aspiration via 0.50 mm ID sample probe and sample capillary. Trace metals of interest were measured under medium resolution (R=4200).

Cytokine analysis—Infected whole hearts were harvested 24 hours post infection, immediately frozen on dry ice, and stored at −80°C prior to analysis. Hearts were spiked with protease inhibitor cocktail (Sigma, St. Louis MO), thawed, and placed in Navy Bullet Blender tubes (Next Advance, Averill Park NY) in 200 μL PBS (Sigma). Hearts were homogenized at 4°C using setting 8 for 4 min and setting 10 for 2 min in the Bullet Blender (Next Advance, Averill Park NY). Beads and cells were pelleted at 4000 x *g* for 10 minutes at 4°C for 10 min and supernatants were collected. Protein concentrations in the

supernatants was quantified by BCA assay kit (Thermo Fisher Scientific, Waltham, MA) and normalized to 10 mg/mL. Cytokines were assayed in supernatants using MILLIPLEX MAP Mouse Cytokine/Chemokine Magnetic Bead Panel (Millipore, Darmstadt, Germany; catalog number: MCYTOMAG-70K) according to the manufacturer's instructions. Samples were run on the Luminex Flexmap 3D platform (Luminex, Austin TX).

Western blotting—Whole hearts were placed in individual Navy Bullet Blender tubes (Next Advance) with 400 μL PBS containing 1% SDS and 1% mammalian protease inhibitor cocktail (Sigma). Hearts were homogenized and lysed twice at 4°C and setting 12 for 5 min each on the Bullet Blender (Next Advance). Debris and beads were pelleted at 16,000 x *g* and 4°C for 10 min. Protein in the supernatants was quantified by BCA assay kit (Thermo). Lysate samples were diluted to 1 mg/mL, combined with 1% 2-mercaptoethanol and loading buffer to 1X, and incubated 15 min at 90°C. Protein, 18 μg per sample, was separated at constant voltage by SDS-PAGE on a 4–20% gel (Bio-Rad). Gels were transferred to nitrocellulose as described by the manufacturer using a Trans-Blot Turbo (Bio-Rad). The blot was blocked rocking at 25°C for 30 min in 4 mL Odyssey blocking buffer (LI-COR), and rocked overnight at 4°C in primary antibodies diluted in 4 mL Odyssey blocking buffer. Primary antibodies, anti-S100A8 from rabbit host (Abcam, ab92331) and anti-Sod1 from goat host (Abcam, ab62800) were both diluted 1:1000. Blots were washed thrice at 25°C in 5 mL PBST, then 1 h at 25°C in secondary antibody diluted in 4 mL Odyssey blocking buffer, then thrice again at 25°C in 5 mL PBST. Secondary antibodies, anti-goat IRDye 680LT (LI-COR, 926-68024) and anti-rabbit IRDye 800CW (LI-COR, 926-32213) were both diluted 1:4000. The blot was developed on the Odyssey system scanning at 700 nm for goat and 800 nm for rabbit.

Flow cytometry—Freshly harvested hearts were dissected in DMEM (Corning, Corning NY) containing 10% FBS (Atlanta Biologicals, Flowery Branch GA) and digested in 10 mg/mL collagenase Type II (Worthington, Lakewood NJ), 2.5 mM $CaCl_2$, 2.4 U/mL dispase II (Sigma, St. Louis MO) for 7 minutes at 37°C. Digested tissue was passed through a 100 μM cell strainer, red blood cells were lysed, and the cell suspension was treated with Fc block (BD Pharmingen, Franklin Lakes NJ). Cells were strained with combinations of the following fluorophore conjugated antibodies: CD45.2 brilliant violet 421 (Biolegend, San Diego CA), CD45.1 brilliant violet 510 (Biolegend, San Diego CA), CD11c PE (BD Pharmingen, Franklin Lakes NJ), Ly6G FITC (BD Pharmingen, Franklin Lakes NJ), F4/80 APC (Invitrogen, Waltham MA), and CD11b PE-Cy7 (Biolegend, San Diego CA). Live/dead was detected using propidium iodide or LIVE/DEAD Fixable Violet Dead Cell Stain Kit (ThermoFisher, Waltham MA). Flow cytometry was conducted on an LSR II (BD, Franklin Lakes NJ).

Calprotectin disc diffusion assay—The purpose of this assay was to determine whether *S. aureus* could bind and utilize calprotectin that is Mn-saturated as a Mn source, building on our previous work demonstrating that calprotectin sequesters Mn and inhibits growth (Corbin et al., 2008; Kehl-Fie et al., 2011; Damo et al., 2013). Disc diffusion assays were modified from published *Neisseria meningitidis* studies (Stork et al., 2013). Solid medium was prepared from Roswell Park Memorial Institute (RPMI) 1640 (Gibco, Thermo

Fisher Scientific, Waltham, MA) containing 1% casamino acids (BD Pharmingen, Franklin Lakes NJ), 2% bacto agar (BD Pharmingen, Franklin Lakes NJ), and 10 μM N,N,N',N'-tetrakis(2-pyridinylmethyl)-1,2-ethanediamine (TPEN, Sigma, St. Louis, MO). TPEN was included to ensure that any growth in the presence of Mn-loaded calprotectin occurred through direct metal transfer. RPMI agar plates were overlaid with soft agar (0.8%) containing 10 μM TPEN and 200 μL (approximately 2×10^7 C.F.U.) or 20 μL (approximately 2×10^8 C.F.U.) of *S. aureus* Newman overnight culture. Subsequently, the soft agar was spotted with 1 μL $MnCl_2$ (100 mM), 5 μL calprotectin + Mn (4 mg/mL), 5 μL calprotectin ΔS1/ΔS1 + Mn (4 mg/mL) (Damo et al., 2013), or 5 μL calprotectin WT (4 mg/mL). Recombinant calprotectin was prepared using a previously established protocol (Kehl-Fie et al., 2011; Damo et al., 2013). In short, recombinant S100A8 and S100A9 are denatured from inclusion bodies with 4 M guanidine hydrochloride, refolded together using dialysis and subsequently purified to form the S100A8/A9 complex. For calprotectin + Mn, S100A8/A9 was dialyzed with excess Mn in dialysis buffer. Plates were photographed after incubation at 37°C for 16 hours. Experiments were performed three times.

Human neutrophil killing assays—Neutrophils were suspended in RPMI (Corning, Corning NY) supplemented with 10 mM 4-(2-hydroxyethyl)-1-piperazineethanesulfonic acid (HEPES) (Corning, Corning, NY) and 0.05% human serum albumin (SeraCare, Milford, MA), medium in which this assay was performed. Flat-bottom 96-well tissue culture treated plates were pre-treated with 20% human serum (SeraCare, Milford, MA) at 37°C and 5% CO_2 for 30 minutes after which hPMNs were seeded at 5×10^5 cells per well. The hPMNs were incubated with 20 μg/ml Apocynin at 37°C and 5% CO_2 for 10 minutes prior to addition of bacteria. Bacteria were grown to mid-logarithmic phase in TSB +/− 1 mM $MnCl_2$ and pre-opsonized with 20% freshly isolated human serum for 30 minutes at 37°C under shaking conditions. Fresh human serum was prepared by drawing blood from 10 consented healthy volunteers under the Torres lab IRB approved protocol (NYU IRB protocol i14-02129) in Serum Separation tubes (BD Vacutainer™). After blood clotting, serum was collected, pooled, and stored at −80°C, as described (Berends et al., 2013). After incubation, bacteria were washed twice and then added to the neutrophils at multiplicity of infection (MOI) of 10 in the absence or presence of 1 mM $MnCl_2$. The plates were centrifuged at 1500 rpm for 5 minutes at 4°C (synchronization) and then incubated at 37°C and 5% CO_2 for 1h. After incubation, the hPMNs were lysed with 0.1% saponin on ice for 15 minutes, then serially diluted in PBS and plated onto TSA for enumeration of surviving colony-forming units (CFU) after overnight incubation. Data are represented as percentage of growth control (wells lacking hPMNS).

Reactive oxygen species measurements

Luminol: Freshly isolated human neutrophils were suspended in Hanks' balanced salt solution (HBSS, Gibco) with 0.1% human serum albumin. In a 96-well black microplate with clear bottom (Corning), 1×10^5 human neutrophils and 50 μM 5-amino-2,3-dihydro-l, 4-phthalazinedione (Luminol, Sigma-Aldrich) in the absence or presence of 1 mM $MnCl_2$ were combined and equilibrated to 37°C. In a total volume of 200 μl/well, 25 nM Phorbol-12-myristate-13-acetate (PMA, EMD Millipore Calbiochem) was added to

stimulate the neutrophils. After 10 minutes incubation at 37°C + 5% CO_2, luminescence was measured by using the EnVision plate reader (PerkinElmer).

Intracellular ROS: Neutrophil ROS was measured by Total Reactive Oxygen Species (ROS) Assay Kit 520 nm (Cat 88-5930, ThermoFisher, Waltham MA) according to the manufacturer's instructions. Freshly isolated human neutrophils (1×10^5/well) were incubated in 1X assay stain solution in a round-bottomed 96-well plate (Corning, Corning NY) for 1 hour at 37°C + 5% CO_2. Following incubation, cells were treated with 25 nM phorbol-12-myristate-13-acetate (PMA, EMD Millipore Calbiochem) +/− 1 mM $MnCl_2$ for 10 minutes at 37°C + 5% CO_2. Cells were fixed with 2% paraformaldehyde and fluorescence of the cells was assessed by flow cytometry (CytoFLEX, Beckman Coulter). Data were analyzed using FlowJo Software (Version 10.1).

Phagocytosis assay—*S. aureus* Newman transformed with pOS1 with the superfolder GFP driven by the *sarA* promoter and *sod* ribosomal binding site (Newman pOS1-pSarA-sodRBS-sGFP) was grown to mid-logarithmic phase and pre-opsonized with human serum, as done for the neutrophil killing experiments, or incubated in medium only as a negative control. Freshly isolated human neutrophils were suspended in RPMI (Corning, Corning NY), 10 mM HEPES (Corning, Corning NY) and 0.05% human serum albumin (SeraCare, Milford, MA) at a concentration of 5×10^6/mL. In a round-bottom plate, 25 μl of neutrophils and pre-opsonized bacteria were combined at an MOI of 10 in the presence or absence of 1 mM $MnCl_2$. The plate was incubated for 15 minutes at 37°C under shaking conditions after which the samples were fixed by adding 2% paraformaldehyde. Samples were analyzed by flow cytometry (CytoFLEX, Beckman Coulter). Neutrophils were gated based on forward side scatter properties and the uptake of *S. aureus* by neutrophils was measured by fluorescence in the FITC channel. Data were analyzed using FlowJo Software (Version 10.1).

Experimental Design

Sample size determination: Sample sizes were not determined a priori by power analysis.

Rules for stopping data collection: Endpoints were defined prior to experiment initiation. Except otherwise noted, animal infections were terminated four days post-infection. Mice that were defined as moribund by veterinary staff blinded to the experimental groups were humanely euthanized and considered to meet the mortality endpoint.

Data inclusion/exclusion criteria: All data collected were included in analyses; animals that did not survive to the endpoint were not assayed. *Outliers.* Outliers were included in analyses, except for rare outliers that resulted from documented experimental error (i.e. infectious inoculum was not properly introduced into the bloodstream).

Replicates: Animal experiments were performed a minimum of two times and data were pooled, with the exception of the timecourse infection, *Tlr-4*$^{-/-}$ and *Ager*$^{-/-}$ infections, and Δ*sodA/M* infection of neutrophil-depleted mice. Growth curves were performed a minimum of three times; independent biological replicates were sampled in technical triplicate.

Randomization: All animals were randomly assigned to diet and treatment groups using random list generator at random.org. Samples from all groups were processed at the same time and using identical techniques. For all animal experiments, groups were labeled by number for analyses and were only decoded after data analysis.

Blinding: Initial diet studies, including survival studies, were performed with the investigator blinded until the completion of the study and data analyses. Subsequent studies were not blinded.

QUANTIFICATION AND STATISTICAL ANALYSIS

Statistical Analysis—Specific statistical details for each experiment can be found in the corresponding figure legend. Sample sizes are specifically noted in each figure legend as appropriate and each experiment was performed at least in biological triplicate. Statistical significance between two groups was examined by a two-tailed Student's *t*-test or the Mann-Whitney test. Statistical significance between survival curves was determined by the log-rank test. Statistical significance between multiple groups was examined by the one-way analysis of variance (ANOVA) with Dunnett's, Sidak's, or Tukey's multiple comparisons test as indicated in the figure legend. Statistical significance between neutrophil killing with or without Mn was determined using a repeated measures ANOVA with Sidak's multiple comparisons test. Statistical work was performed using Prism 6 software (GraphPad) and a P value of less than 0.05 was considered significant. Details related to inclusion/exclusion criteria, randomization, and sample size determination can be found under experimental design in the methods details section.

DATA AND SOFTWARE AVAILABILITY

Microbiota 16S Sequencing—All FASTQ sequence data obtained in this study has been deposited to the Sequence Read Archive (SRA) at NCBI with the accession number SRP097779.

Supplementary Material

Refer to Web version on PubMed Central for supplementary material.

Acknowledgments

We thank the Skaar laboratory for critical insight into this project and helpful feedback on the manuscript and Jacob Choby, Lauren Palmer, Brittany Nairn, Catherine Wakeman, Michael Noto, Andrew Monteith and Neal Hammer for assistance in animal experiments. We acknowledge the Vanderbilt Flow Cytometry Shared Resource and Margaret Allaman for technical assistance. Work in E.P.S.'s laboratory was supported by Public Health Service Grants AI101171, AI107233, AI069233, and AI073843, Veterans Affairs grant INFB-024-13F, Vanderbilt Digestive Disease Research Center (VDDRC) (grant no. P30DK058404), and the Defense Advanced Research Projects Agency (DARPA). Work in R.M.C.'s laboratory was supported by Public Health Service Grant 6P41 GM103391-06. L.J.J. was supported by American Heart Association Grant 15PRE25060007 and Public Health Service award T32 GM07347 from the National Institute of General Medical Studies for the Vanderbilt Medical-Scientist Training Program. Work in V.J.T.'s laboratory was supported by Public Health Service Grants AI099394, AI105129, AI103268 and HHSN272201400019C. V.J.T. is a Burroughs Wellcome Fund Investigator in the Pathogenesis of Infectious Diseases. E.T.M.B was supported by a Rubicon fellowship from the Netherlands Organization for Scientific Research. J.P.Z. was supported by NIH–NIDDK grant no. T32DK007673 and NIH–NIAID grant no. F32AI120553.

References

Anderson DJ, Moehring RW, Sloane R, Schmader KE, Weber DJ, Fowler VG Jr, Smathers E, Sexton DJ. Bloodstream infections in community hospitals in the 21st century: a multicenter cohort study. PLOS One. 2014; 9:e91713. [PubMed: 24643200]

Benson MA, Lilo S, Nygaard T, Voyich JM, Torres VJ. Rot and SaeRS cooperate to activate expression of the staphylococcal superantigen-like exoproteins. J Bacteriol. 2012; 194:4355–4365. [PubMed: 22685286]

Berends ET, Dekkers JF, Nijland R, Kuipers A, Soppe JA, van Strijp JA, Rooijakkers SH. Distinct localization of the complement C5b-9 complex on Gram-positive bacteria. Cell Microbiol. 2013; 15:1955–1968. [PubMed: 23869880]

Brinkmann V, Zychlinsky A. Beneficial suicide: why neutrophils die to make NETs. Nat Rev Microbiol. 2007; 5:577–582. [PubMed: 17632569]

Btaiche IF, Carver PL, Welch KB. Dosing and monitoring of trace elements in long-term home parenteral nutrition patients. J Parenter Enteral Nutr. 2011; 35:736–747.

Cheng AG, Kim HK, Burts ML, Krausz T, Schneewind O, Missiakas DM. Genetic requirements for *Staphylococcus aureus* abscess formation and persistence in host tissues. FASEB J. 2009; 23:3393–3404. [PubMed: 19525403]

Cho H, Jeong DW, Liu Q, Yeo WS, Vogl T, Skaar EP, Chazin WJ, Bae T. Calprotectin Increases the Activity of the SaeRS Two Component System and Murine Mortality during *Staphylococcus aureus* Infections. PLOS Pathog. 2015; 11:e1005026. [PubMed: 26147796]

Corbin BD, Seeley EH, Raab A, Feldmann J, Miller MR, Torres VJ, Anderson KL, Dattilo BM, Dunman PM, Gerads R, et al. Metal chelation and inhibition of bacterial growth in tissue abscesses. Science. 2008; 319:962–965. [PubMed: 18276893]

Damo SM, Kehl-Fie TE, Sugitani N, Holt ME, Rathi S, Murphy WJ, Zhang Y, Betz C, Hench L, Fritz G, et al. Molecular basis for manganese sequestration by calprotectin and roles in the innate immune response to invading bacterial pathogens. Proc Nat Acad Sci. 2013; 110:3841–3846. [PubMed: 23431180]

Dhople AM, Ibanez MA, Poirier TC. Role of iron in the pathogenesis of *Mycobacterium avium* infection in mice. Microbios. 1996; 87:77–87. [PubMed: 9032957]

Diaz-Ochoa VE, Lam D, Lee CS, Klaus S, Behnsen J, Liu JZ, Chim N, Nuccio SP, Rathi SG, Mastroianni JR, et al. Salmonella mitigates oxidative stress and thrives in the inflamed gut by evading calprotectin-mediated manganese sequestration. Cell Host Microbe. 2016; 19:814–825. [PubMed: 27281571]

Frosch M, Metze D, Foell D, Vogl T, Sorg C, Sunderkotter C, Roth J. Early activation of cutaneous vessels and epithelial cells is characteristic of acute systemic onset juvenile idiopathic arthritis. Exp Derm. 2005; 14:259–265. [PubMed: 15810883]

Garcia YM, Barwinska-Sendra A, Tarrant E, Skaar EP, Waldron KJ, Kehl-Fie TE. A superoxide dismutase capable of functioning with iron or manganese promotes the resistance of *Staphylococcus aureus* to calprotectin and nutritional immunity. PLOS Pathog. 2017; 13:e1006125. [PubMed: 28103306]

Greger JL. Dietary standards for manganese: overlap between nutritional and toxicological studies. J Nutr. 1998; 128:368S–371S. [PubMed: 9478027]

Hauser RA, Zesiewicz TA, Rosemurgy AS, Martinez C, Olanow CW. Manganese intoxication and chronic liver failure. Ann Neurol. 1994; 36:871–875. [PubMed: 7998773]

Hood MI, Mortensen BL, Moore JL, Zhang Y, Kehl-Fie TE, Sugitani N, Chazin WJ, Caprioli RM, Skaar EP. Identification of an *Acinetobacter baumannii* zinc acquisition system that facilitates resistance to calprotectin-mediated zinc sequestration. PLOS Pathog. 2012; 8:e1003068. [PubMed: 23236280]

Hood MI, Skaar EP. Nutritional immunity: transition metals at the pathogen-host interface. Nat Rev Microbiol. 2012; 10:525–537. [PubMed: 22796883]

Horsburgh MJ, Wharton SJ, Cox AG, Ingham E, Peacock S, Foster SJ. MntR modulates expression of the PerR regulon and superoxide resistance in *Staphylococcus aureus* through control of manganese uptake. Mol Microbiol. 2002a; 44:1269–1286. [PubMed: 12028379]

Horsburgh MJ, Wharton SJ, Karavolos M, Foster SJ. Manganese: elemental defence for a life with oxygen. Trends Microbiol. 2002b; 10:496–501. [PubMed: 12419613]

Hung TH, Hsieh YH, Tseng KC, Tsai CC, Tsai CC. The risk for bacterial endocarditis in cirrhotic patients: a population-based 3-year follow-up study. Int J Infect Dis. 2013; 17:e391–393. [PubMed: 23352807]

Jean S, Juneau RA, Criss AK, Cornelissen CN. *Neisseria gonorrhoeae* evades calprotectin-mediated nutritional immunity and survives neutrophil extracellular traps by production of TdfH. Infect Immun. 2016; 84:2982–2994. [PubMed: 27481245]

Jonker FA, Boele van Hensbroek M. Anaemia, iron deficiency and susceptibility to infections. J Infect. 2014; 69(Suppl 1):S23–27. [PubMed: 25264159]

Juttukonda LJ, Chazin WJ, Skaar EP. *Acinetobacter baumannii* coordinates urea metabolism with metal import to resist host-mediated metal limitation. mBio. 2016:7.

Juttukonda LJ, Skaar EP. Manganese homeostasis and utilization in pathogenic bacteria. Mol Microbiol. 2015; 97:216–228. [PubMed: 25898914]

Katona P, Katona-Apte J. The interaction between nutrition and infection. Clin Infect Dis. 2008; 46:1582–1588. [PubMed: 18419494]

Kehl-Fie TE, Chitayat S, Hood MI, Damo S, Restrepo N, Garcia C, Munro KA, Chazin WJ, Skaar EP. Nutrient metal sequestration by calprotectin inhibits bacterial superoxide defense, enhancing neutrophil killing of *Staphylococcus aureus*. Cell Host Microbe. 2011; 10:158–164. [PubMed: 21843872]

Kehl-Fie TE, Zhang Y, Moore JL, Farrand AJ, Hood MI, Rathi S, Chazin WJ, Caprioli RM, Skaar EP. MntABC and MntH contribute to systemic *Staphylococcus aureus* infection by competing with calprotectin for nutrient manganese. Infect Immun. 2013; 81:3395–3405. [PubMed: 23817615]

Kelliher JL, Kehl-Fie TE. Competition for manganese at the host-pathogen interface. Prog Mol Biol Transl Sci. 2016; 142:1–25. [PubMed: 27571690]

Klein M, Wang A. Infective Endocarditis. J Intensive Care Med. 2016; 31:151–163. [PubMed: 25320158]

Le Moing V, Alla F, Doco-Lecompte T, Delahaye F, Piroth L, Chirouze C, Tattevin P, Lavigne JP, Erpelding ML, Hoen B, et al. *Staphylococcus aureus* bloodstream infection and endocarditis--a prospective cohort study. PLOS One. 2015; 10:e0127385. [PubMed: 26020939]

Lisher JP, Giedroc DP. Manganese acquisition and homeostasis at the host-pathogen interface. Front Cell Infect Microbiol. 2013; 3:91. [PubMed: 24367765]

Mann DL. Inflammatory mediators and the failing heart: past, present, and the foreseeable future. Circ Res. 2002; 91:988–998. [PubMed: 12456484]

Moore CM, Helmann JD. Metal ion homeostasis in *Bacillus subtilis*. Curr Opin Microbiol. 2005; 8:188–195. [PubMed: 15802251]

Palmer LD, Skaar EP. Transition metals and virulence in bacteria. Ann Rev Genet. 2016; 50:67–91. [PubMed: 27617971]

Pruenster M, Kurz AR, Chung KJ, Cao-Ehlker X, Bieber S, Nussbaum CF, Bierschenk S, Eggersmann TK, Rohwedder I, Heinig K, et al. Extracellular MRP8/14 is a regulator of beta2 integrin-dependent neutrophil slow rolling and adhesion. Nat Commun. 2015; 6:6915. [PubMed: 25892652]

Radin JN, Kelliher JL, Parraga Solorzano PK, Kehl-Fie TE. The two-component system ArlRS and alterations in metabolism enable *Staphylococcus aureus* to resist calprotectin-induced manganese starvation. PLOS Pathog. 2016; 12:e1006040. [PubMed: 27902777]

Rahil-Khazen R, Bolann BJ, Myking A, Ulvik RJ. Multi-element analysis of trace element levels in human autopsy tissues by using inductively coupled atomic emission spectrometry technique (ICP-AES). J Trace Elem Med Biol. 2002; 16:15–25. [PubMed: 11878748]

Reyes-Robles T, Lubkin A, Alonzo F 3rd, Lacy DB, Torres VJ. Exploiting dominant-negative toxins to combat Staphylococcus aureus pathogenesis. EMBO Rep. 2016; 17:780. [PubMed: 27139260]

Rigby KM, DeLeo FR. Neutrophils in innate host defense against *Staphylococcus aureus* infections. Semin Immunopathol. 2012; 34:237–259. [PubMed: 22080185]

Ryckman C, Vandal K, Rouleau P, Talbot M, Tessier PA. Proinflammatory activities of S100: proteins S100A8, S100A9, and S100A8/A9 induce neutrophil chemotaxis and adhesion. J Immunol. 2003; 170:3233–3242. [PubMed: 12626582]

Schloss PD, Westcott SL, Ryabin T, Hall JR, Hartmann M, Hollister EB, Lesniewski RA, Oakley BB, Parks DH, Robinson CJ, et al. Introducing mothur: open-source, platform-independent, community-supported software for describing and comparing microbial communities. Appl Environ Microbiol. 2009; 75:7537–7541. [PubMed: 19801464]

Sikk K, Haldre S, Aquilonius SM, Asser A, Paris M, Roose A, Petterson J, Eriksson SL, Bergquist J, Taba P. Manganese-induced parkinsonism in methcathinone abusers: bio-markers of exposure and follow-up. Eur J Neurol. 2013; 20:915–920. [PubMed: 23347399]

Spraggins JM, Rizzo DG, Moore JL, Rose KL, Hammer ND, Skaar EP, Caprioli RM. MALDI FTICR IMS of Intact Proteins: Using Mass Accuracy to Link Protein Images with Proteomics Data. Journal Am Soc Mass Spec. 2015; 26:974–985.

Stork M, Grijpstra J, Bos MP, Manas Torres C, Devos N, Poolman JT, Chazin WJ, Tommassen J. Zinc piracy as a mechanism of *Neisseria meningitidis* for evasion of nutritional immunity. PLOS Pathog. 2013; 9:e1003733. [PubMed: 24204275]

Tong SY, Davis JS, Eichenberger E, Holland TL, Fowler VG Jr. *Staphylococcus aureus* infections: epidemiology, pathophysiology, clinical manifestations, and management. Clin Microbiol Rev. 2015; 28:603–661. [PubMed: 26016486]

Vogl T, Tenbrock K, Ludwig S, Leukert N, Ehrhardt C, van Zoelen MA, Nacken W, Foell D, van der Poll T, Sorg C, et al. Mrp8 and Mrp14 are endogenous activators of Toll-like receptor 4, promoting lethal, endotoxin-induced shock. Nat Med. 2007; 13:1042–1049. [PubMed: 17767165]

Weinberg ED. Nutritional immunity. Host's attempt to withold iron from microbial invaders. JAMA. 1975; 231:39–41. [PubMed: 1243565]

Weinberg ED. Iron availability and infection. Biochim et Biophysica Acta. 2009; 1790:600–605.

Yan L, Bjork P, Butuc R, Gawdzik J, Earley J, Kim G, Hofmann Bowman MA. Beneficial effects of quinoline-3-carboxamide (ABR-215757) on atherosclerotic plaque morphology in S100A12 transgenic ApoE null mice. Atherosclerosis. 2013; 228:69–79. [PubMed: 23497784]

Yang J, Caprioli RM. Matrix sublimation/recrystallization for imaging proteins by mass spectrometry at high spatial resolution. Anal Chem. 2011; 83:5728–5734. [PubMed: 21639088]

Zackular JP, Moore JL, Jordan AT, Juttukonda LJ, Noto MJ, Nicholson MR, Crews JD, Semler MW, Zhang Y, Ware LB, et al. Dietary zinc alters the microbiota and decreases resistance to *Clostridium difficile* infection. Nat Med. 2016; 22:1330–1334. [PubMed: 27668938]

Highlights

- High levels of dietary manganese increase lethality and heart colonization by *S. aureus*
- Calprotectin does not alter manganese availability in the heart
- Mice fed a high manganese diet have increased bioavailable manganese in the heart
- *S. aureus* utilizes dietary manganese to protect against ROS and neutrophil killing

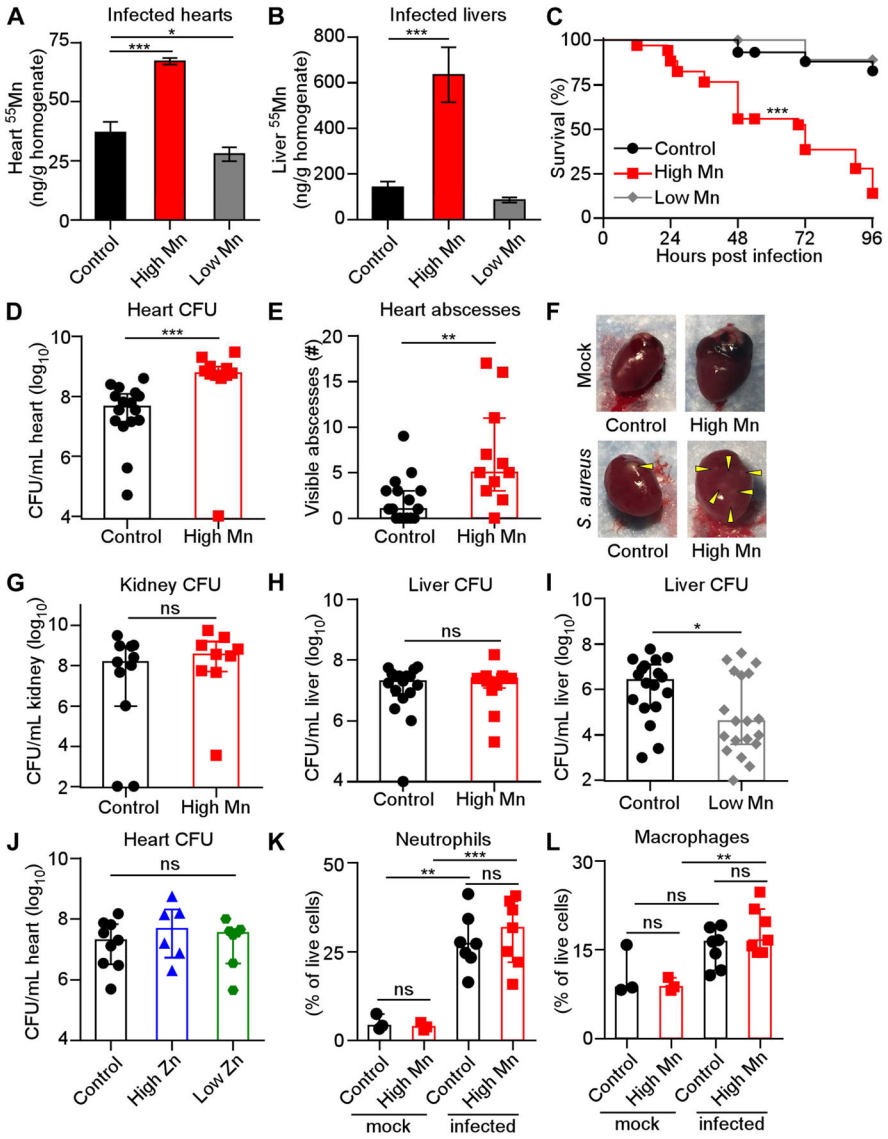

Figure 1. High Mn diet increases lethality and heart bacterial burdens from *S. aureus* systemic infection

WT mice were fed modified diets and infected with *S. aureus* for four days (**A–J**) or 18 hours (**K–L**). (**A–B**) Mn concentrations in (**A**) heart homogenates and (**B**) liver homogenates were measured by ICP-MS. $N = 3$. **(C)** Survival was monitored. Low Mn $N = 10$; control $N = 29$; high Mn $N = 34$. **(D)** CFU present in heart homogenates. For (**D–E)** and (**H),** $N = 16$ (control), 11 (high Mn). **(E)** Enumeration of heart abscesses. (**F)** Heart appearance. Arrowheads indicate abscesses. (**G**) CFU present in kidney homogenates. $N = 11$ (control); $N = 9$ (high Mn). (**H**) CFU present in liver homogenates. (**I**) CFU present in liver homogenates. $N = 18$ (control); $N = 19$ (low Mn). (**J**) CFU present in heart homogenates from mice fed modified Zn diets. $N = 7$ (high Zn, low Zn), 9 (control). (**K–L**) Flow cytometry quantification of immune cells in the heart. Previous gate: live cells. $N = 7$ (infected), $N = 3$ (mock). (**K**) Neutrophils, Ly6G+ CD11b+. (**L**) Macrophages, F4/80+. (**A–B**) Bars depict mean and SEM. (**D–E, G–L**) Bars depict median and interquartile range. ns =

not significant. *$P < 0.05$. ** $P < 0.01$. *** $P < 0.001$ by log-rank test (**C**), Mann-Whitney test (**D, E, G–I**) or one-way analysis of variance (ANOVA) with Dunnett's multiple comparisons test (**A–B**) or Tukey's multiple comparisons test (**J–L**). See also Figure S1.

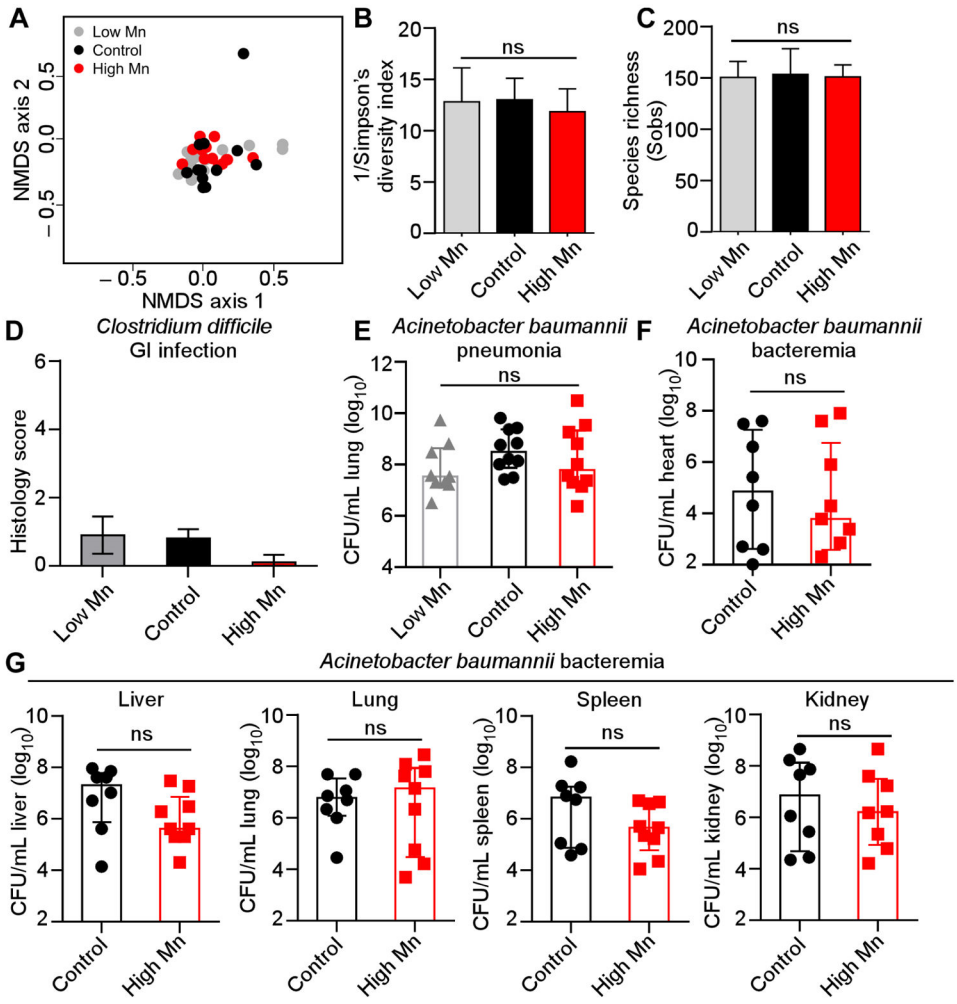

Figure 2. Dietary Mn does not alter the gut microbiota or impact infection with *Clostridium difficile* or *Acinetobacter baumannii*

(A–C) Microbiota analysis during a 4-week time course of dietary Mn manipulation. (**A**) Nonmetric multidimensional scaling (NMDS) ordination showing gut microbiota β-diversity. Distances were measured using the Yue and Clayton index of dissimilarity (θ_{YC}). No significant differences were observed between groups (Analysis of Molecular Variance; AMOVA) ($P > 0.05$). (**B**) Inverse Simpson's diversity for each diet. (**C**) Species richness measured by Sobs (number of observed OTUs) for each diet. (**D**) Blinded histological scores from ceca were determined 4 days post-infection with *C. difficile*. Error bars represent standard deviation. (**E**) CFU recovered from lungs 36 hours following intranasal inoculation with *A. baumannii*. (**F–G**) CFU recovered from (**F**) heart and (**G**) liver, lungs, spleen and kidney 24 hours following intravenous inoculation with *A. baumannii*. (**E–G**) Bars indicate median +/− interquartile range. ns = not significant by ANOVA with Tukey's multiple comparison's test (**E**) or Mann-Whitney (**F, G**).

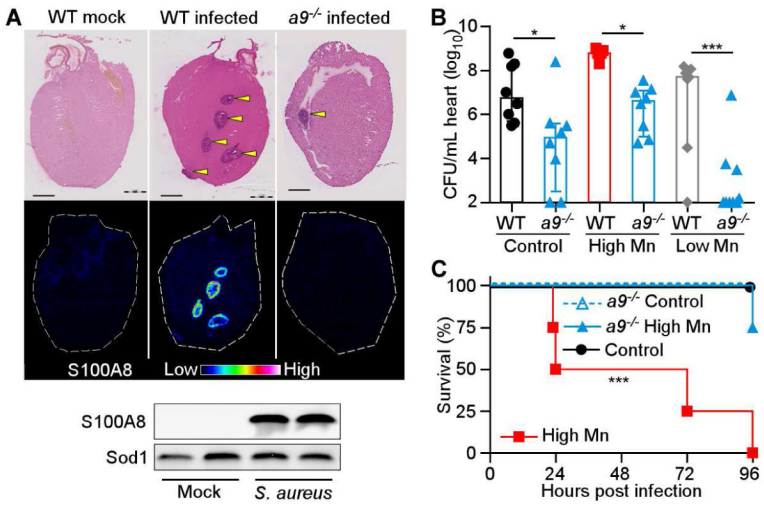

Figure 3. Calprotectin enhances *S. aureus* infection of the heart

(**A–C**) *S100a9*$^{-/-}$ (*a9*$^{-/-}$) or WT mice were fed high Mn, control, or low Mn diet and mock-infected or infected with *S. aureus* for 4 days. **(A)** MALDI-MS images of S100A8 from hearts of mice fed high Mn diet. Top, H&E stained section. Arrowheads indicate abscesses. Scale bar is 1 mm. Below, immunoblot for Sod1 (loading control) and S100A8 in hearts from WT mice. Images and blots are representative of three independent experiments. **(B)** Heart bacterial burdens recovered from WT and *S100a9*$^{-/-}$ mice. $N = 8$ (control WT, control *a9*$^{-/-}$, high Mn *a9*$^{-/-}$), 5 (high Mn WT), 7 (low Mn WT), 9 (low Mn *a9*$^{-/-}$). Bars show median +/− interquartile range. **(C)** Survival of WT and *S100a9*$^{-/-}$ mice following infection. $N = 4$. Survival is representative of three independent experiments. *$P < 0.05$, *** $P < 0.001$ by ANOVA with Tukey's multiple comparisons test **(B)** or log-rank test **(C).** See also Figure S2

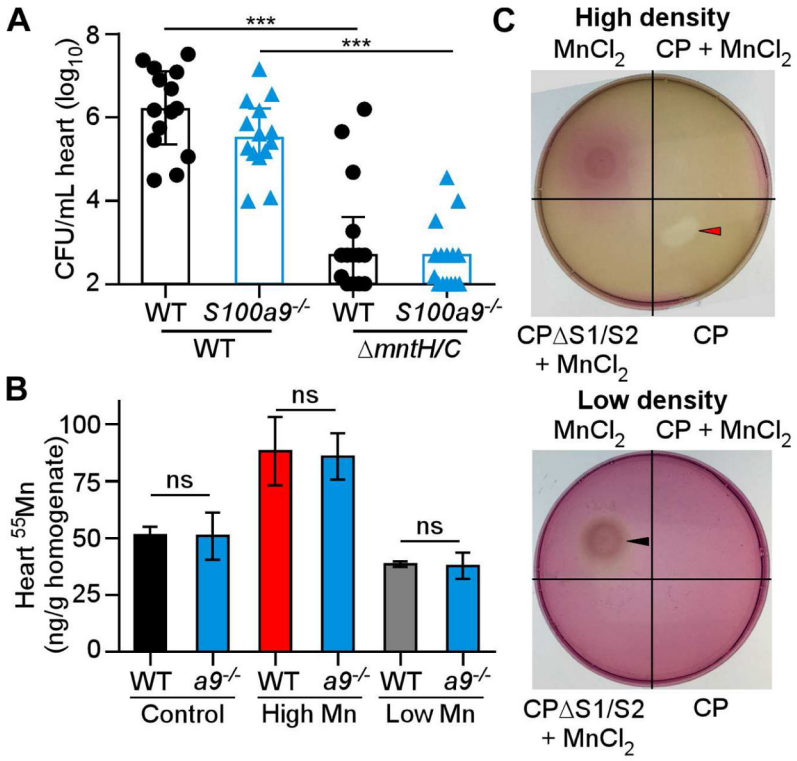

Figure 4. Loss of calprotectin does not impact Mn bioavailability in the heart

(**A**) Heart bacterial burdens from WT and *S100a9*$^{-/-}$ mice provided normal chow and infected for 4 days with *S. aureus* WT or Δ*mntH*/*C*. $N = 15$ (*S100a9*$^{-/-}$ Δ*mntH*/*C*), $N = 14$ (all other groups). (**B**) Mn concentrations in heart homogenates, measured by ICP-MS. Hearts are from infected WT or *S100a9*$^{-/-}$ (*a9*$^{-/-}$) mice fed high Mn, control, or low Mn diet. $N = 3$. (**C**) *S. aureus* growth on RPMI agar containing 10 μM TPEN spotted with CP or $MnCl_2$ sources as labeled. Number of bacteria plated: high density = 2×10^8 CFU, low density = 2×10^7 CFU. Red arrow = growth inhibition, black arrow = growth enhancement. **(A)** Bars depict median and interquartile range. **(B)** Bars depict mean and SEM. *** $P < 0.001$, ns = not significant by ANOVA with Sidak's multiple comparisons test. See also Figure S3.

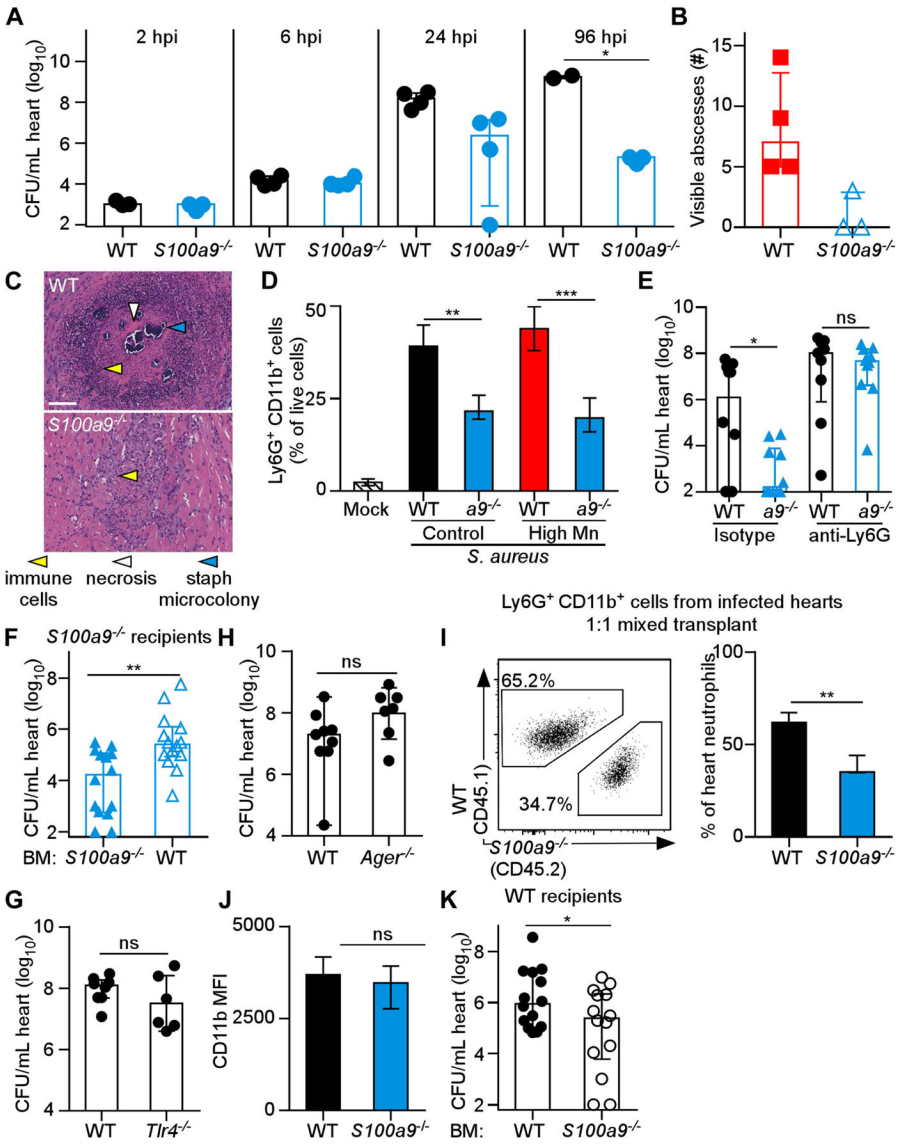

Figure 5. Calprotectin supports *S. aureus* infection of the heart while promoting neutrophil recruitment

Mice were placed on high Mn diet (**A, B, D**) or control diet (**C–K**) for 5–8 weeks and infected with WT *S. aureus* for various timepoints (**A**) or four days (**B–K**). (**A**) Heart bacterial burdens. $N = 3$ (2 hour, *S100a9*$^{-/-}$ 96 hour); $N = 4$ (4 and 24 hour); $N = 2$ (WT 96 hour). (**B**) Heart abscesses. $N = 4$ (WT); $N = 3$ (*S100a9*$^{-/-}$). (**C**) Histopathology of infected hearts. Scale bar is 100 μM. **(D)** Flow cytometry quantification of Ly6G^{+}CD11b^{+} cells from hearts. Previous gate, live cells. $N = 4$ (high Mn groups), 3 (control groups), 2 (mock). (**E**) Heart bacterial burdens following treatment with anti-Ly6G or isotype control antibodies. $N = 9$ (WT depleted), 10 (all other groups). (**F**) Heart bacterial burdens from *S100a9*$^{-/-}$ mice transplanted with WT or *S100a9*$^{-/-}$ bone marrow (BM). (**G–H**) Heart bacterial burdens from WT and *Tlr4*$^{-/-}$ mice (**G**) or *Ager*$^{-/-}$ mice (**H**). (**I**) Ly6G^{+}CD11b^{+} cells following BM transplantation of a 1:1 mix of WT congenic BM (CD45.1) and *S100a9*$^{-/-}$ BM (CD45.2) into WT mice. Previous gate, CD45^{+} cells. Left, representative flow plot. Right,

quantification of neutrophil percentages. $N = 3$. (**J**) Mean fluorescence intensity of CD11b on Ly6G$^+$ WT and *S100a9*$^{-/-}$ cells. $N = 7$ (WT), 5 (*S100a9*$^{-/-}$). (**K**) Heart bacterial burdens from WT mice transplanted with WT or *S100a9*$^{-/-}$ BM. (**A–K**) Bars depict median and interquartile range. ns, not significant; *, $P < 0.05$; **, $P < 0.01$; ***, $P < 0.001$ by Mann-Whitney (**A, D**); unpaired *t*-test (**E–K**). See also Figures S3 & S4.

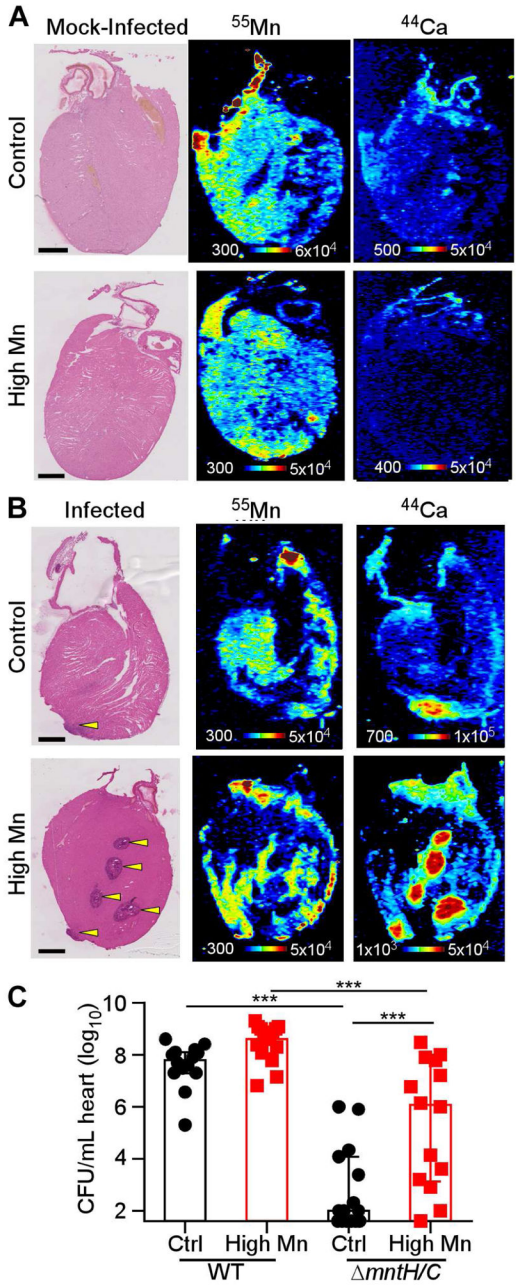

Figure 6. Excess dietary Mn is bioavailable to *S. aureus* in the heart

WT mice were fed high Mn or control diet and infected mock-infected with PBS (**A**) or infected with *S. aureus* WT (**B**) for 4 days. The arrangement and relative concentrations of Mn and Ca in heart sections were assessed by LA-ICP-MS. Left, H&E stained serial sections. Scale bar is 1 mm. (**C**) Heart bacterial burdens from infection with WT or Δ*mntH/C*. $N = 14$ (Control WT, high Mn Δ*mntH/C*); 15 (control Δ*mntH/C,* high Mn WT). Bars are median +/− interquartile range. *** $P < 0.001$ by ANOVA with Tukey's multiple comparisons test. See also Figure S2.

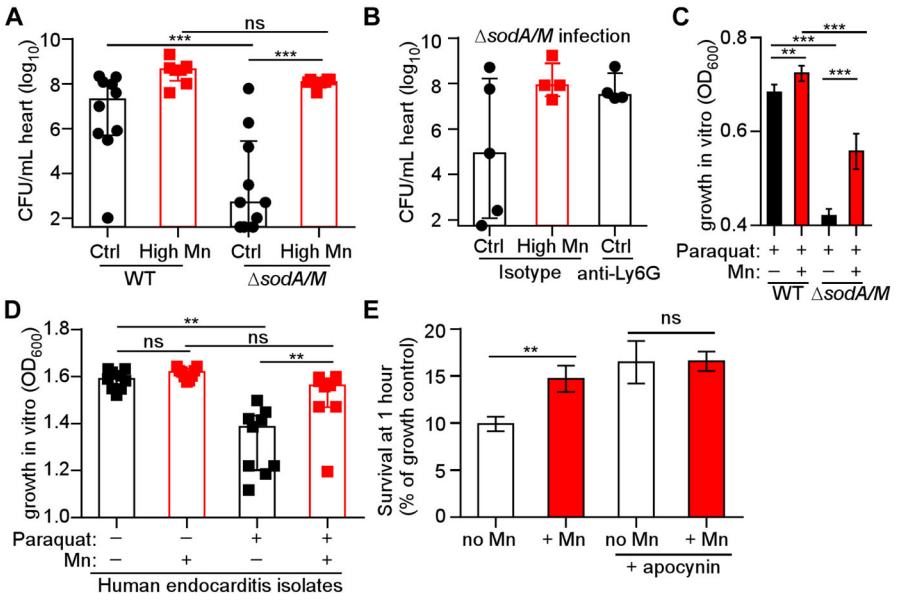

Figure 7. Excess dietary Mn protects against reactive oxygen species *in vivo*

WT mice were fed high Mn or control diet and infected with *S. aureus* or Δ*sodA/M* for four days. (**A**) Heart bacterial burdens. $N = 10$ (control diet groups), 8 (high Mn diet groups). (**B**) Heart bacterial burdens of Δ*sodA/M* following treatment with anti-Ly6G antibody or isotype control. $N = 5$ (control diet, isotype group) or 4 (other groups). (**C**) Growth of *S. aureus* WT or Δ*sodA/M* in 1 mM paraquat and 1 mM $MnCl_2$. OD_{600} was measured at 8 hours. Data are combined from three independent experiments. (**D**) Growth of 9 clinical endocarditis isolates in 5 mM paraquat and 1 mM $MnCl_2$. Each symbol represents an independent bacterial isolate. OD_{600} was measured at 21 hours. (**E**) Bacterial survival (% growth control) after 1 hour incubation of *S. aureus* with human neutrophils +/− 1 mM $MnCl_2$. Apocynin treatment was used to inhibit neutrophil NADPH oxidase. $N = 14$ donors. **(A–B, D)** Bars depict median and interquartile range. (**C, E**) Bars depict mean and SEM. * $P < 0.05$. ** $P < 0.01$. *** $P < 0.001$ by ANOVA with Tukey's multiple comparisons (**A–C**), repeated measures ANOVA with Tukey's multiple comparisons test (**D**), or repeated measures ANOVA with Sidak's multiple comparisons (**E**). See also Figures S5 & S6.